Novel Role of Endothelial CD45 in Regulating Endothelial-to-Mesenchymal Transition in Atherosclerosis

Qianman Peng[1†], Kulandaisamy Arulsamy[2†], Yao Wei Lu[1,2,6†], Bo Zhu[1], Bandana Singh[1], Kui Cui[1], Jill Wylie-Sears[1], Marina V. Malovichko[4], Scott Wong[1], Douglas B. Cowan[1], Masanori Aikawa[3], Sanjay Srivastava[4], Da-Zhi Wang[2,5], Joyce Bischoff[1]*, Kaifu Chen[2]*, Hong Chen[1]*

1. Vascular Biology Program, Boston Children's Hospital, and Department of Surgery, Harvard Medical School, Boston, Massachusetts, USA.
2. Department of Cardiology, Boston Children's Hospital, and Department of Pediatrics, Harvard Medical School, Boston, Massachusetts,USA.
3. Center for Interdisciplinary Cardiovascular Sciences, Brigham and Women's Hospital, and Department of Medicine, Harvard Medical School, Boston, MA,USA.
4. Department of Medicine, University of Louisville, Louisville, Kentucky,USA.
5. Center for Regenerative Medicine, USF Health Heart Institute, Department of Internal Medicine, University of South Florida, Tampa, Florida, USA.
6. Department of Medicine and Hastings Center for Pulmonary Research, Keck School of Medicine, University of Southern California, Los Angeles, California, USA.

†These authors contributed equally to this work.

*Correspondence to: hong.chen@childrens.harvard.edu
kaifu.chen@childrens.harvard.edu
joyce.bischoff@childrens.harvard.edu

ABSTRACT

Background: The protein tyrosine phosphatase CD45 is expressed in all nucleated cells of the hematopoietic system and in mitral valve endothelial cells (ECs) undergoing endothelial-to-mesenchymal transition (EndoMT). Our recent work indicated that activation of endogenous CD45 in human endothelial colony-forming cells (ECFCs) induced expression of multiple EndoMT marker genes. We hypothesized that CD45 may contribute to atherosclerosis; however, detailed molecular mechanisms underlying how CD45 may contribute to EndoMT and the impact of therapeutic manipulation of CD45 expression in atherosclerosis are unknown.

Methods: We generated a tamoxifen-inducible EC-specific CD45-deficient mouse strain (EC-iCD45KO) on an ApoE-deficient (WT/ApoE$^{-/-}$) background and fed them a Western diet (WD) to produce atherosclerosis. We enriched mouse aortic ECs with anti-CD31 beads to perform single-cell RNA sequencing. Cellular, biochemical and molecular approaches were used to investigate the effect of endothelial CD45-specific deletion on EndoMT and lesion development in an ApoE$^{-/-}$ mouse model of atherosclerosis.

Results: EC-iCD45KO mice showed reductions in lesion development, plaque macrophage infiltration, and expression of cell adhesion molecules when compared to WT/ApoE$^{-/-}$ controls. Single-cell RNA sequencing revealed that loss of endothelial CD45 decreases EndoMT marker expression and TGF-β signaling in atherosclerotic mice, which is associated with reduction of lesions. Mechanistically, CD45 loss increases Fibroblast Growth Factor Receptor 2 (FGFR2) expression in mouse aortic ECs and Krüppel-like Factor 2 (KLF2) expression in the aortic root. Endothelial CD45-deficiency also inhibits EndoMT and TGFβ signaling in atherosclerosis.

Conclusions: Our findings demonstrate that genetic depletion of endothelial CD45 protects against EndoMT-driven atherosclerosis by promoting FGFR2 and KLF2 expression while inhibiting Transforming Growth Factor beta (TGFβ) signaling and EndoMT. Consequently, targeting endothelial CD45 may represent a novel therapeutic strategy to reduce EndoMT in atherosclerosis.

Key words: Atherosclerosis; Endothelial CD45; Endothelial-to-Mesenchymal Transition (EndoMT); Single-cell Analysis; TGF-β Signaling.

INTRODUCTION

Accumulating evidence indicates that CD45 (*PTPRC*), the prototypic receptor-like protein tyrosine phosphatase (PTP), is an essential regulator of signal transduction in hematopoietic cells. It dephosphorylates phosphotyrosine residues to dampen cell signaling[1]. While CD45 is not commonly expressed in endothelial cells (ECs), lung ECs have been found to express CD31 and CD45 in a pulmonary arterial hypertension rat model[2]. Notably, we recently reported that activation of the endogenous CD45 promoter in human endothelial colony forming cells (ECFCs) induced expression of endothelial-to-mesenchymal transition (EndoMT) markers and increased cell migration, contraction of collagen gels, and permeability consistent with EndoMT[3]. In addition, a CD45 phosphatase inhibitor blocked EndoMT in Transforming Growth Factor beta 1 (TGFβ1)-treated ovine mitral valve ECs[4]. These findings led us to speculate that endothelial CD45-specific deletion may prevent EndoMT-driven atherosclerosis.

Atherosclerosis is the leading cause of morbidity and mortality in the United States and most developed countries[5]. Endothelial dysfunction caused by cholesterol and oxidized phospholipids in lipoproteins (*e.g.*, oxidized Low Density Lipoprotein or oxLDL) are major atherosclerosis-initiating events[6]. Trapped lipoproteins activate ECs and vascular smooth muscle cells (VSMCs) to increase expression of adhesion molecules and chemokines[7]. This leads to recruitment of monocytes/lymphocytes into the arterial wall[8]. Lesion progression involves the migration and proliferation of resident smooth muscle cells (SMCs)[9], extracellular matrix deposition[8], and lipid or necrotic core formation[10]. In advanced stages of atherosclerosis, there is increased endothelial dysfunction and advanced plaque ruptures associated with thin, collagen-poor fibrous caps[11] that can result in myocardial infarctions and ischemic strokes.

EndoMT is an incremental process where ECs progressively lose endothelial-specific markers and properties while gaining mesenchymal attributes[12]. ECs can be distinguished by expression of specific endothelial genes in normal physiological conditions. For example, ECs express platelet/EC adhesion molecule-1 (CD31/PECAM-1), vascular endothelial (VE)-cadherin, and von Willebrand factor, which are reduced during EndoMT[13]. At the same time, transitioning ECs express mesenchymal markers such as αSMA, collagen, and SM22[14]. While EndoMT plays a fundamental role in forming cardiac valves of the heart development, there is mounting evidence that EndoMT is involved in atherosclerosis in adults[15,16].

TGFβ signaling is a central player in driving EndoMT during atheroma progression[17] but the processes leading to its activation are poorly defined. TGFβ signaling in ECs during EndoMT

results in expression of pro-inflammatory chemokines and cytokines as well as their receptors[17], leukocyte adhesion molecules (*e.g.*, ICAM-1 and VCAM-1)[18], and extracellular matrix (ECM) components linked to inflammation[8]. In contrast, a non-inflammatory EC phenotype can be preserved through FGFR signaling, which counteracts TGFβ-driven EndoMT[19]. Reductions in endothelial FGFR-mediated signaling enhances TGFβ signaling leading to EndoMT[20]. Endothelial FGFR1 and the regulatory transcription factor Krüppel-like Factor 2 (KLF2) are reduced by inflammation[21], whereas FGFR2 activation can enhance autocrine FGF2 production, which has been shown to improve cardiac function in infarcted mice[22].

The objective of this study was to establish if endothelial CD45-specific deletion could prevent EndoMT in atherosclerosis. To do this, we generated tamoxifen-inducible EC-specific CD45-deficient mice (EC-iCD45KO) on an ApoE$^{-/-}$background then fed these mice an atherosclerotic Western diet (WD). We performed single-cell RNA sequencing (scRNA-seq) and biochemical experiments to assess endothelial CD45-mediated TGFβ- and FGF-receptor signaling *in vitro* and *in vivo*. Our findings demonstrate that loss of endothelial CD45 protects against EndoMT-driven atherosclerosis, while simultaneously promoting FGFR2 and KLF2 expression and inhibiting TGFβ signaling and EndoMT marker expression. These studies strongly indicate that endothelial CD45 may represent a novel drug target for the treatment of atherosclerosis.

MATERIALS AND METHODS

Additional Materials and Methods are available in the Supplemental Materials and Methods and Supplemental Tables.

Genetic Mouse Models and Aortic Lesion Evaluation

All animal procedures were performed in compliance with institutional guidelines, and mouse protocols were approved by the Institutional Animal Care and Use Committee (IACUC) of Boston Children's Hospital. Both male and female mice were used, including C57BL/6 mice (Jax stock #00664), ApoE$^{-/-}$ mice (Jax stock #002052), and EC-specific Cre deleter mice (iCDH5CreERT2) (The Jackson Laboratory). Please see the Supplemental Materials and Methods for a description of the breeding scheme. Tamoxifen-inducible deletion of endothelial CD45 on an ApoE$^{-/-}$ background (EC-iCD45KO/ApoE$^{-/-}$) was accomplished by performing 7 injections every other day as previously described[23]. For controls, C57BL/6 iCDH5 CreERT2 mice were denoted as wild-type (WT). These mice were crossed onto an ApoE$^{-/-}$ background to obtain control ApoE$^{-/-}$/WT (WT/ApoE$^{-/-}$) mice. WT/ApoE$^{-/-}$ and EC-iCD45KO/ApoE$^{-/-}$ were fed a Western diet (WD) for 12-16 weeks beginning at 8 months of age. We evaluated atherosclerotic lesions at the aortic sinus, abdominal aorta, and thoracic aorta. Mice were perfused, dissected, and subjected to quantification of atherosclerosis as previously described[24].

Cell Culture

To isolate murine aortic ECs (MAECs), aortas were collected and washed twice with PBS at 4°C and then stripped of fat and connective tissue[23,24]. Aortas were cut into 3 mm long sections, and segments were put on the Matrigel-coated (Corning) plate with EC medium[25]. After 4 days, vascular networks were visible under the light microscope and tissue segments were removed. ECs were detached and cultured in fresh endothelial medium. The identity of isolated ECs was confirmed by immunofluorescence staining for the EC marker CD31. A full list of reagents including antibodies and primers is included in the Supplemental Tables. Cultured MAECs isolated from EC-iCD45KO/ApoE$^{-/-}$ iCDH5-Cre mice were treated with 5 μM tamoxifen for 3 days to induce deletion of CD45. MAECs isolated from ApoE$^{-/-}$ mice were treated in parallel with tamoxifen to serve as controls. Cells were treated with 100 μg/mL oxLDL or 10 ng/mL TGFβ1 while maintaining 2 μM tamoxifen in the medium.

Aortic Sample Preparation for scRNA-seq

Aortic cells were isolated as described previously[23]. Mouse aortas were cut into fine pieces and

109 placed in 5 mL of enzyme solution at 37°C. Supernatants were collected every 10 min until all
110 pieces were digested (Enzyme solution: 5 mL of DMEM, Collagenase type I: 5mg/mL (Gibco),
111 Collagenase type IV: 5mg/mL (Gibco), Liberase:5mg/mL (Roche)). Supernatants were filtered
112 with a 40-µm strainer, centrifuged at 400g for 5 mins, and the cell pellet was suspended in 90
113 µL of buffer containing 0.5% BSA and 2 mmol/L EDTA in PBS. Then, 20 µL of CD31
114 microbeads (Miltenyi Biotec) was added to the suspension at 4° C for 15 mins. Microbeads
115 were passed through an MS column (Miltenyi Biotec). Cells were processed for scRNA-seq
116 with the 10x Genomics platform and sequencing was performed by MedGenome (**Figure S1**).

117 **Profiling Single-Cell Transcriptomes Using 10X scRNA-sequencing**

118 The raw sequence reads from WT/ApoE$^{-/-}$ and EC-iCD45KO/ApoE$^{-/-}$ samples were obtained
119 using 10X Genomics scRNA-seq and processed independently. These reads were aligned
120 against the mouse reference genome (mm10) using Cell Ranger[26] (version 7.1.0). This pipeline
121 generated a gene expression count matrix, with rows representing genes and columns
122 representing individual cells. Subsequently, we employed the Seurat R package (version
123 5.1.0)[27] for downstream analysis. Low-quality cells were excluded if they had fewer than 500
124 or more than 4500 expressed genes, or if the percentage of mitochondrial or ribosomal reads
125 exceeded 5% or 16%, respectively. For each sample, doublet cells identified by the
126 DoubletFinder[28] program were removed. The remaining high-quality cells were then subjected
127 to log normalization, data scaling, principal component analysis (PCA), and cell clustering.
128 Cell clustering and sub-clustering were performed using the FindClusters and FindSubCluster
129 functions, respectively. Marker genes for each cluster were identified using the FindAllMarkers
130 function, with a minimum percentage of expressed cells set at 25% and a minimum log2 fold
131 change of 0.25. These marker genes were used to annotate cell types based on known markers
132 from public databases[29,30] and the literature[23]. Differentially expressed genes between
133 WT/ApoE$^{-/-}$ and EC-iCD45KO/ApoE$^{-/-}$ samples were analyzed by grouping cells from each
134 sample by the interested cell types (EndoMT1 and EndoMT2) and running the FindMarkers
135 function. For pathway enrichment analysis, we utilized the clusterProfiler R package[31] to
136 explore the Gene Ontology (GO) pathways of differentially regulated genes. In case of data
137 visualization, we utilized the DimPlot for UMAP plots, and VlnPlot and DotPlot functions for
138 plotting gene expression levels across different cell types between samples. The Wilcoxon non-
139 parametric test was used to calculate p-values for single-cell gene expression analysis, and a
140 proportion test was applied to assess the statistical significance of differences in cell type
141 proportions between WT/ApoE$^{-/-}$ and EC-iCD45KO/ApoE$^{-/-}$ groups. We utilized the SCIG

142 tool[32] to characterize cell identity genes across cell types in both groups, followed by Gene
143 Ontology (GO) pathway analysis to investigate their functional roles. Further, we analyzed
144 human single-cell RNA-seq data from healthy controls and atherosclerosis samples[33,34] to
145 assess the expression of CD45/PTPRC and other endothelial functional genes such as CDH5,
146 EMCN, and FLT1 in Pecam1-expressing cells.

147 **Single-Cell Trajectory, RNA Velocity, and Cell–Cell Communication Analyses**

148 To investigate the role of CD45 in the EndoMT process, we performed single-cell cellular
149 dynamics analysis using RNA velocity, implemented with the scVelo Python package. In this
150 approach, the future states of individual cells were modeled based on the ratio of unspliced and
151 spliced mRNA transcripts abundance[35]. Trajectory inference analysis for each sample was
152 conducted using the R package monocle3[36]. Changes in gene expression along trajectories were
153 visualized with the R ComplexHeatmap[37] package. We investigated cell-cell communication
154 by identifying potential ligands in sender cells and their corresponding target genes in receiver
155 cells using the nichenetr package[38]. To understand which cell-cell communication signals
156 regulate the EndoMT process, we specifically performed the analysis by considering EndoMT
157 cells as sender cells and ECs as receiver cells.

158 **Hematoxylin and Eosin Staining**

159 Cryostat sections of the mouse aortic root, abdominal aorta, and brachiocephalic artery (BCA)
160 were washed in PBS for 5 mins, then fixed in 4% paraformaldehyde for 15 mins. Slides were
161 stained with hematoxylin for 3 mins, followed by running tap water washes for 10 mins. Slices
162 were then dipped in eosin working solution for 30 seconds, rinsed with tap water, and
163 dehydrated using graded ethanol (95% and 100% ethanol), followed by treatment with xylenes.
164 Slices were mounted in synthetic resin as previously described[39].

165 **Flow Cytometry**

166 Flow cytometry analysis of aortic cells from normal diet (ND) ApoE$^{-/-}$ and WD diet ApoE$^{-/-}$
167 (16-20 weeks) was performed on cells isolated as described above. Cell pellets were
168 resuspended in FACS buffer (2% HBSS, 0.004% FBS, 2mM EDTA in PBS) at 4°C for 30 min
169 to block nonspecific binding of antibodies to Fc receptors. Cells were incubated with antibodies
170 for 30 mins and flow cytometry analyses were performed using a BD instrument.

171 **Oil Red O Staining**

172 Cryostat sections were fixed in 4% paraformaldehyde[23,39]. Slides were washed with PBS, and
173 rinsed with 60% isopropanol, followed by staining with freshly prepared 0.5% Oil Red O
174 solution in isopropanol for 20 mins at 37°C[39]. Slices were then put in 60% isopropanol for 30
175 seconds, followed by 3 washes in water, and dried slides were mounted with glycerin. Imaging
176 was performed using a Zeiss LSM880 microscope and analyzed with ZEN-Lite software and
177 NIH ImageJ software.

178 Whole aortae were dissected symmetrically, pinned to parafilm for *en face* exposure and fixed
179 in formalin for 24 hrs. Aortae were washed in PBS three times and rinsed in 100% propylene
180 glycol, followed by staining with 0.5% Oil Red O solution in propylene glycol for 20 mins at
181 65°C. The samples were then put in 85% propylene glycol for 2 mins, followed by three washes
182 in distilled water and then dried. Imaging was performed using a Nikon SMZ1500
183 stereomicroscope, SPOT Insight 2Mp Firewire digital camera, and SPOT Software 5.1.

184 **RNA Isolation and Quantitative Real-time PCR**

185 Total RNA was extracted from primary MAECs using RNeasy kits (Qiagen)[24]. On-column
186 DNA digestion (Qiagen) was carried out during RNA extraction. For the synthesis of the first
187 strand of cDNA, 1 μg of total RNA after DNase treatment was reverse transcribed using cDNA
188 Synthesis Kit (Vazyme). Quantitative real-time PCR was performed on a CFX96 detection
189 system (StepOnePlus Real-Time PCR Systems) with SYBR Green reagents (Vazyme). All
190 PCR primer sequences are presented in the Supplemental Tables.

191 **Evaluation of EndoMT Markers by Immunostaining *In Vivo* and *In Vitro***

192 Samples from ApoE$^{-/-}$ and EC-iCD45KO/ ApoE$^{-/-}$ mice were evaluated by co-staining CD31
193 (or VE-Cadherin) with α-SMA, KLF2, and ICAM-1. EndoMT is expressed by the overlapping
194 percentile of CD31 (or VE-Cadherin) with other markers. For *in vitro* EndoMT marker staining,
195 mouse aortic EC (MAEC) cultures were treated with oxLDL (100 μg/mL) or TGFβ1 (10 ng/mL)
196 or TGFβ1 (5ng/mL) on the indicated days.

197 **Immunofluorescence Staining**

198 *Human Tissue Paraffin Sections*: Human healthy control and diseased aortic arch samples from
199 atherosclerosis patients were purchased from Maine Medical Center Biobank (Sample ID:
200 RA06-1040A1)[24]. The paraffin sections were de-paraffinized and subjected to antigen retrieval
201 to unmask antigenic epitopes with 10 mM Sodium Citrate, pH 6.0, and 0.5% Tween 20 at 90 °C
202 for 30 mins[23]. Immunofluorescence staining of slides was performed using the protocol

203 described below. Samples were blocked in PBS with donkey serum, 3% BSA, and 0.3% Triton
204 X-100 at 4°C overnight and incubated with primary antibodies VE-Cadherin with CD45 at 4°C
205 overnight[40]. Sections were washed three times, and respective secondary antibodies conjugated
206 to fluorescent labels (Alexa Flour 594, 488, or 647) were added for 2 hrs at room temperature.
207 Sections were mounted with Fluoroshield (R&D Systems) mounting medium containing DAPI
208 (1:100).

209 *Mouse aortic root and BCA cryosections*: Sections were fixed with 4% paraformaldehyde for
210 15 min at room temperature and blocked in PBS solution containing 3% donkey and/or 10%
211 goat serum, 3% BSA, and 0.3% Triton X-100 for 1 hr[23,39]. Samples were then incubated with
212 primary antibody at 4°C overnight, followed by incubation with respective secondary
213 antibodies conjugated to fluorescent labels (Alexa Flour 594, 488, or 647; 1:200) for 2 hrs at
214 room temperature. Sections were mounted with Fluoroshield (R&D Systems) mounting
215 medium containing DAPI (1:100).

216 ***En Face* Preparation and Immunofluorescent Labeling**

217 *En face* immunofluorescence was performed as described[41]. Thoracic aortae were isolated and
218 fixed in 2% paraformaldehyde solution at 4 °C for 1.5 hrs. Fixed tissues were permeabilized in
219 PBS containing 0.2% Triton X-100 (permeabilization buffer) for 1 hr at room temperature and
220 incubated with a blocking buffer (5.5% FBS in permeabilization buffer) for 1 hr at room
221 temperature. Primary antibodies were diluted in staining buffer (2.75% FBS in
222 permeabilization buffer) and incubated with tissue for 16 hrs at 4 °C with gentle agitation.
223 Tissues were washed 3× in permeabilization buffer in 30-min intervals. Secondary antibodies
224 (conjugated with Alexa Fluor 647, Alexa Fluor 594, or Alexa Fluor 488) diluted as a 1:200
225 working solution (10 μg/mL) in the staining buffer were added after the third wash and
226 incubated at room temperature for 3 hrs. Tissues were washed 3× in permeabilization buffer
227 and 1× in PBS for 30 mins at each step. After the PBS wash, vascular tissues were bisected
228 along the direction of flow and mounted with Fluoroshield (R&D Systems). Images were
229 obtained using a Zeiss LSM 880 microscope and Zen Black software. Zen Blue software was
230 used for image export and analysis. Unless specified, secondary antibodies for
231 immunohistochemistry were applied at a concentration of 1:200.

232 **Data Analysis**

233 For relative gene expression data (qPCR) analysis, we use the Livak-Schmittgen method
234 ($2^{-\Delta\Delta Cq}$), which compares two values in the exponent that represent the normalized

235 expression values for a gene of interest in samples relative to Actin or CDH5 between WT and
236 EC-iCD45 KO cells[42]. For immunofluorescence (IF) staining, the extracted nucleus regions
237 were split into isolated nuclei before counting using DAPI staining. Two-tailed unpaired
238 Student's t-tests were applied to EC-iCD45KO/ApoE$^{-/-}$ and WT/ApoE$^{-/-}$ atherosclerotic mice.
239 Data are expressed as the mean ± SEM. The means of two groups were compared using
240 Student's t-test (unpaired, two-tailed) with $P < 0.05$ considered to be statistically significant.
241 The lipid panel test was analyzed by Column Statistics and data are expressed as the mean ±
242 SE. Unless indicated, all experiments were repeated at least three times. All data were analyzed
243 by Prism 8 (GraphPad Software).

RESULTS

CD45 Expression in the Endothelium of Atherosclerotic Lesions

We first determined if CD45 was present in the endothelium of the aortic arch in pathological specimens from human patients with atherosclerosis. We detected CD45 in VE-Cadherin^{+} cells in aortic arch samples from patients with severe and mild atherosclerotic lesions (**Figure 1A**). By analyzing publicly available human scRNA-seq profiles, we observed that CD45 mRNA expression was upregulated in atherosclerosis patients compared to healthy controls **(Figure 1B**). In contrast, genes that maintain normal endothelial function such as CDH5, EMCN and FLT1 were downregulated in ECs from atherosclerotic samples (**Figure 1B**). These data suggest that upregulation of CD45 is associated with endothelial dysfunction.

As ApoE$^{-/-}$ mice fed a normal diet also develop lesions, albeit at a slower rate compared to WD-fed ApoE$^{-/-}$ mice, we chose to use WT mice that were fed normal chow as our true negative control for atherosclerosis occurrence to rule out the potential effect of high cholesterol content in WD-fed mice and lesion development in normal chow-fed ApoE$^{-/-}$ mice (**Figure 1C**). When comparing aortas from ApoE$^{-/-}$ mice fed a normal diet versus WD, lesions were apparent in ApoE$^{-/-}$ WD-fed aortas. Flow cytometric analyses of total aortic cells for VE-Cadherin, FGFR1 and CD45 showed a significant reduction in VE-Cadherin^{+}/FGFR1^{+} ECs in WD-fed ApoE$^{-/-}$ mice, compared to normal diet-fed ApoE$^{-/-}$ mice (**Figure 1D** and **1E**). In contrast, VE-Cadherin^{+}/CD45^{+} ECs were increased in WD-fed ApoE$^{-/-}$ mice compared to normal diet-fed ApoE$^{-/-}$ mice, suggesting loss of FGFR1 may contribute to EndoMT in lesions of WD-fed ApoE$^{-/-}$ mice (5.5 vs 16.3%, $p = 0.0324$).

We generated mice with tamoxifen-inducible deletion of endothelial CD45 on an ApoE$^{-/-}$ background (EC-iCD45KO/ApoE$^{-/-}$) (**Figure 1F** and **Figure S1A**,**B**). Mice from either genotype fed a WD diet for 16 weeks (WT/ApoE$^{-/-}$) showed no difference in body weight for males or females (data not shown). Serum total cholesterol and triglycerides measurements (124.2.8±28.46 vs 103.6 ± 19.02; p value = 0.6700); HDL (73.27 ± 13.99 vs 79.44 ± 18.03; p value = 0.9270, LDL (728.6 ± 111.9 vs 762.4 ± 117.4; $p = 0.5516$), showed no significant difference between WT/ApoE$^{-/-}$ and EC-iCD45KO/ApoE$^{-/-}$ mice (**Figure S2**). We then analyzed expression and localization of CD45 in mouse aortic ECs by immunofluorescence staining of sections from the aortic root. CD45 was detected and co-expressed with CD31 in 12-week-old ApoE-null mice (**Figure 1G** and **1H**). Intriguingly, there was a significant decrease in CD45 in ECs from EC-iCD45KO/ApoE$^{-/-}$ mice (~52.05%; $p = 0.0028$). Aortas

276 from WT/ApoE$^{-/-}$ mice fed a WD showed more lesions when compared to EC-
277 iCD45KO/ApoE$^{-/-}$ WD-fed aortas (male, 16-week WD) (**Figure 1I**). Consistent with this
278 observation, whole-mount *en face* aortas from female WT/ApoE$^{-/-}$ and EC-iCD45KO/ApoE$^{-/-}$
279 mice stained with Oil Red O after a 16-week WD had a reduction in lesion size (~36.78%; p =
280 0.0176) (**Figure 1J** and **1K**). Together, these results show that CD45 depletion significantly
281 reduces atherosclerotic burden in ApoE-null mice.

282 **Single-Cell Profiling Shows CD45 Deletion Suppresses EndoMT and Reshapes Vascular**
283 **Cell Identity in Atherosclerosis**

284 To establish that endothelial CD45 plays a decisive role in atherosclerosis progression, we
285 profiled single-cell transcriptomes of atherosclerotic ApoE$^{-/-}$ and EC-iCD45KO/ApoE$^{-/-}$ mice
286 using scRNA-seq and bioinformatic analyses. WT/ApoE$^{-/-}$ and EC-iCD45KO/ApoE$^{-/-}$ male
287 mice were fed a WD for 16 weeks, followed by isolation of aortas, enzymatic digestion,
288 scRNA-seq and data analysis (**Figure S1C**). Through stringent data preprocessing, we retained
289 high-quality cells by filtering based on the number of genes expressed, doublets as well as
290 mitochondrial and ribosomal gene expression signatures (**Figure S3A**). We also integrated
291 single-cell datasets from WT/ApoE$^{-/-}$ and EC-iCD45KO/ApoE$^{-/-}$ mice, corrected for batch
292 effects and subsequently performed single-cell clustering and downstream analyses. We
293 confirmed the efficacy of CD45 knockout in aortic ECs (**Figure S3B**) using single-cell
294 transcriptomic profiles.

295 Through our single-cell data analysis, we identified 25 distinct clusters, which were grouped
296 into major cell types (**Figure S3C**, left**)**, including vascular cells (*e.g.*, ECs and VSMCs) and
297 immune cells (*e.g.*, macrophages, B cells, T cells and others). We then focused on vascular
298 cells to investigate the association of CD45 with the EndoMT process (**Figure S3C**, right).
299 Within this subset, we identified five vascular cell types based on their marker gene expression
300 signatures (**Figure 2A**): ECs (Pecam1, Cdh5), EndoMT1 cells (Fbln5, Fbln2), EndoMT2 cells
301 (Tgfb1, Tgfbr2), VSMCs (Acta2, Tagln), and proliferating cells (Top2a, Mki67) (**Figure S3D**).

302 Comparative analysis of cell populations in WT/ApoE$^{-/-}$ and EC-iCD45KO/ApoE$^{-/-}$ aortas
303 revealed a significant increase in the EC population (from 14% to 28%) and a reduction in
304 vascular SMCs (from 58% to 53%) in EC-iCD45KO/ApoE$^{-/-}$ mice compared to ApoE$^{-/-}$ mice
305 (**Figure 2B**). We characterized EndoMT cells into two subclusters—EndoMT1 and EndoMT2
306 (**Figure 2A**). In the EndoMT cell clusters, the population of EndoMT1 (~3%) and EndoMT2
307 (~9%) significantly decreased in the EC-iCD45KO group (**Figure 2B**). These findings suggest

308 that the loss of CD45 in ECs contributes to rewiring of vascular cell identity and function in
309 atherosclerotic ApoE$^{-/-}$ mice.

310 Next, we compared the gene expression signatures in EndoMT cell types between two groups
311 (*i.e.*, EC-iCD45KO/ApoE$^{-/-}$ and WT/ApoE$^{-/-}$ mice). Violin plots showed that EC function genes
312 (Cdh5, Flt1, Mecom) were upregulated in EC-iCD45KO/ApoE$^{-/-}$ aortas compared
313 with WT/ApoE$^{-/-}$ aortas (**Figure 2C**). At the same time, SMC function genes (Mef2c, pde4d,
314 pdcd4) and EndoMT markers (Fbln2, Fbln5, Clu) were downregulated in EC-iCD45KO/ApoE^{-}
315 $^{/-}$ mice in EndoMT1 cells (**Figure 2D** and **2E**). Similarly, in EndoMT2 cells, EC function genes
316 (Sparc, Bsg, Egr1) increased (**Figure 2F**), but SMC function genes (Mef2c, pde4d, pdcd4) and
317 EndoMT markers (TGFβ1, TGFβR2, Ebf1) decreased in EC-iCD45KO/ApoE$^{-/-}$ mice when
318 compared to WT/ApoE$^{-/-}$ mice (**Figure 2G** and **2H**).

319 **SCIG Analysis Illustrates CD45-Deficiency Reprograms EndoMT Cells Toward an**
320 **Endothelial Identity while Suppressing Mesenchymal and Inflammatory Signatures**

321 Recently, we showed that SCIG[32] effectively profiles the full spectrum of cell identity genes
322 (CIGs) that enables detailed characterization of individual cell types and their functional states
323 in atherosclerotic and control samples[43]. To characterize transcriptomic and functional
324 differences between EndoMT1 and EndoMT2 cells, we identified CIGs using SCIG and
325 performed GO pathway analysis. Unlike differential expression analysis, which compares gene
326 expression between conditions, the SCIG algorithm is designed to uncover CIGs within a given
327 cell type by integrating gene expression values with gene sequence signatures. Genes with an
328 FDR < 0.05 in SCIG predictions were considered potential CIGs. Pearson correlation analysis
329 of CIGs and their scores revealed that EndoMT1 and EndoMT2 cells share substantial cell
330 identity, with a correlation of 0.49 in WT/ApoE$^{-/-}$ mice compared to a reduced correlation of
331 0.26 in EC-iCD45KO/ApoE$^{-/-}$ mice (**Figure 2I**). These findings suggest that EndoMT2 cells
332 underwent the most pronounced transcriptional and cellular changes between the two groups.

333 We further observed that 749 CIGs were shared between EndoMT1 and EndoMT2 cell types
334 (**Figure 2J)**, many of which were implicated in EndoMT-related processes such as EC
335 migration, activation of TGF-β signaling and mesenchymal cell development (**Figure 2K**).
336 Pathway analysis of uniquely enriched CIGs (226 genes) revealed that EndoMT2 cells were
337 functionally associated with immune processes and inflammatory signaling, including B-, T-,
338 and mast cell activation, mononuclear cell proliferation, interleukin production, muscle cell
339 development and inflammatory responses (**Figure S4A**, right). In contrast, unique CIGs in

340 EndoMT1 cells (303 genes) were enriched in pathways primarily associated with inflammatory
341 responses, mesenchymal cell development and EC function (**Figure S4A**, left). Moreover, we
342 observed that CD45 is highly expressed in both EndoMT1 and EndoMT2 cells of WT/ApoE$^{-/-}$
343 mice, suggesting a role for CD45 in regulating EndoMT during atherosclerosis (**Figure S3B**).

344 To investigate the role of CD45 in determining cell identity, we applied the SCIG algorithm to
345 each vascular cell type by identifying CIGs in WT/ApoE$^{-/-}$ and EC-iCD45KO mice. Pearson
346 correlation analysis of CIG scores between the two groups revealed the lowest correlation for
347 EndoMT2 cells ($r = 0.50$), followed by EndoMT1 ($r = 0.68$), VSMCs ($r = 0.79$) and ECs ($r =$
348 0.80) (**Figures 2L** and **S4B**). These results indicate the cell identity of EndoMT1 and EndoMT2
349 populations is more divergent and modulated by CD45 status compared to VSMCs and ECs.

350 Based on these findings, we performed pathway analysis on the uniquely identified CIGs in
351 WT/ApoE$^{-/-}$ and EC-iCD45KO mice for both EndoMT1 and EndoMT2 cells (**Figures 2M**, and
352 **S5A** to **S5G**). Pathways related to mesenchymal development and differentiation, epithelial
353 cell fate, SMC contraction and proliferation as well as cytokine and inflammatory responses
354 were significantly enriched among uniquely identified CIGs in EndoMT1 and EndoMT2 cells
355 from WT/ApoE$^{-/-}$ mice (**Figures S5B** and **S5F**), but not in EC-iCD45KO mice. The endothelial
356 function pathways, including EC proliferation, vascular development, VEGF and WNT
357 signaling and angiogenesis were enriched among uniquely identified CIGs in both EndoMT1
358 and EndoMT2 cells from EC-iCD45KO mice (**Figures S5D** and **S5G**).

359 Additionally, we visualized these pathways through gene concept network diagrams that depict
360 pathway nodes and their connecting gene edges to highlight functional relationships (**Figures**
361 **2M**, **S5C** and **S5E**). For instance, in WT/ApoE$^{-/-}$ mice, EndoMT2 cells showed enrichment of
362 mesenchymal development pathways driven by genes such as Snai2, Smad2 and Pdcd4, along
363 with cytokine receptor activity genes including Il7r, Il2rb, Cxcr5 and Ccr10 (**Figure 2M**, left).
364 In contrast, EC-iCD45KO mice exhibited enrichment of endothelium development and
365 differentiation pathways in EndoMT2 cells with genes such as Kdr, Notch1, Tie2, Tjp2 and
366 Ednrb supporting endothelial function programs (**Figure 2M**, right). Together, these identity
367 gene signatures, and pathway analyses reveal CD45 loss attenuates mesenchymal-like
368 transition programs and promotes endothelial identity and function.

369 **Single-Cell Dynamics Analyses Shows Deletion of Endothelial CD45 Inhibits EndoMT in**
370 **Atherosclerosis**

371 To further study the role of CD45 in EndoMT, we performed single-cell dynamics analysis,

372 which enables the study of how individual cells differentiate into other cells. First, we applied
373 RNA velocity analysis to the cells from each group and found that ECs in WT/ApoE$^{-/-}$ mice
374 exhibited strong transitions toward EndoMT1 and EndoMT2 populations, eventually acquiring
375 a VSMC phenotype (**Figure 3A**, left). In contrast, this transition was markedly reduced in EC-
376 iCD45KO/ApoE$^{-/-}$ mice (**Figure 3A**, right). Trajectory analysis using Monocle3 revealed that
377 in WT/ApoE$^{-/-}$ mice, the inferred trajectory progressed from ECs along two distinct paths,
378 EndoMT1 and EndoMT2, ultimately leading toward VSMCs (**Figure 3B**) when ECs were
379 selected as the root cells. Along this trajectory in WT/ApoE$^{-/-}$ mice, endothelial function genes
380 (Pecam1, Vwf, Kdr) were downregulated, indicating a loss of EC identity, while upregulation
381 of VSMC function genes (Myl9, Acta2, Tagln) suggested a shift toward a VSMC-like
382 phenotype (**Figure 3C** and **3D**).

383 EndoMT1 and EndoMT2 cells represent intermediate states, characterized by upregulation of
384 EndoMT markers (Tgfb1, Bgn, Clu) and inflammatory markers (Tnf, Cxcl2), bridging ECs and
385 VSMCs (**Figure 3C, left)**. In addition, when EndoMT1 or EndoMT2 cells were used as the
386 root, the trajectories also terminated in VSMCs (**Figure S6A** and **S6B**). VSMC function gene
387 expression patterns aligned with the EndoMT process trajectory (**Figure S6C** and **S6D**) in
388 WT/ApoE$^{-/-}$ mice. However, through unbiased RNA velocity analysis, the EndoMT transition
389 was markedly inhibited in EC-iCD45KO mice where VSMCs tended to revert toward an EC-
390 like state (**Figure 3A, right**). Consistent with the RNA velocity results, the inferred trajectory
391 (**Figures 3B, right** and **3D right**) and associated gene expression changes (**Figure 3C, right**)
392 support a VSMC-to-EC transition (MEndoT, Mesenchymal-to-Endothelial Transition). Results
393 from both RNA velocity and trajectory analyses were consistent, demonstrating that EndoMT
394 was prevalent in WT/ApoE$^{-/-}$ mice but significantly suppressed and reversed in EC-iCD45KO
395 mice.

396 **CD45 Drives EndoMT Through Cell-Cell Communication Signals**

397 To identify potential cell-cell communication signals in the EndoMT process, we used the
398 NicheNet tool to prioritize ligands and their target genes based on single-cell expression
399 profiles. In this analysis, EndoMT2 and VSMC cells were designated as sender cells, while
400 ECs served as receiver cells (**Figures 3E** to **3I**). Using the NicheNet pipeline, we identified
401 potential ligands in EndoMT1 cells of WT/ApoE$^{-/-}$ mice, including Ptprc/CD45, Tgfβ1, and in
402 VSMCs (**Figure 3E**, left), including Col18a1, Lum, and Timp1 (**Figure 3E**, left). These ligands
403 were found to regulate target genes such as Irf7, Cav1, Sgk1, and Timp3, which are involved

404 in accelerating EndoMT (**Figure 3F**). Expression levels of the identified target genes were
405 decreased in CD45-deletion mice (**Figure 3H)**. Notably, in CD45-deletion mice, these ligand-
406 target gene signaling interactions were diminished (**Figure 3G)**. We observed the target genes
407 Fos, Atf3, Abca1, Lmna and Runx1 that are involved in endothelial identity, proliferation and
408 cholesterol efflux, were upregulated in CD45-deletion mice (**Figure 3I**).

409 **Endothelial CD45-Deficiency Inhibits EndoMT by Preventing TGFβR Signaling and**
410 **Increasing FGFR2 Expression during Atherosclerosis**

411 We performed *en face* immunofluorescence staining of the thoracic aorta with antibodies to
412 VE-Cadherin, CD31, DAPI and CD45. This showed CD45 co-expression with VE-Cadherin
413 and CD31 in WT ApoE-null mice but a significant reduction of CD45 expression (22.95%; p
414 = 0.0308) in EC-iCD45KO ApoE-null mice (**Figure 4A** to **4C**). Endothelial dysfunction is a
415 critical event in vascular inflammation that is characterized, in part, by elevated cell surface
416 expression of adhesion molecules such as intercellular adhesion molecule-1 (ICAM-1) and
417 vascular adhesion molecule-1 (VCAM-1). Accordingly, we observed a reduction of ICAM-1
418 expression (25.22%;p = 0.0087) in ECs from the thoracic aortas of EC-iCD45KO/ApoE$^{-/-}$ mice
419 and a similar reduction in aortic roots from these mice (**Figure 4D** to **4F** and **S7A**) compared
420 to WT/ApoE$^{-/-}$ mice. In contrast, VCAM1 expression in the aortic root did not show a
421 significant difference between WT/ApoE$^{-/-}$ and EC-iCD45KO/ApoE$^{-/-}$ mice (**Figure S7B**).

422 Because collagen type I alpha 1 (Col1a1) is a crucial structural component of the fibrous cap
423 in atherosclerotic plaques, we assessed the expression of this protein in aortic roots. We found
424 a reduction of Col1a1 immunofluorescence staining in EC-iCD45KO/ApoE$^{-/-}$ mice (**Figure 4**
425 **G**). We also determined that Col1a1 colocalized less with VE-cadherin in EC-iCD45KO/ApoE^{-}
426 $^{/-}$ mice when compared to WT/ApoE$^{-/-}$ mice (38.88%; p = 0.0080) (**Figure 4H** and**4I**). This
427 indicated a reduction of collagen content in ECs in EC-iCD45KO/ApoE$^{-/-}$ mice. In addition,
428 we detected upregulation of KLF2 (1.717-fold; p = 0.0175) in the aortic roots from EC-
429 iCD45KO/ApoE$^{-/-}$ mice fed a WD for 12 weeks when compared to WT/ApoE$^{-/-}$ mice (**Figure**
430 **S8A** and **S8B**). These findings are consistent with our observation that EndoMT cell clusters
431 were functionally associated with immune processes and inflammatory signaling.

432 Our results indicate that loss of endothelial CD45 results in diminished atherosclerosis while
433 TGFβ signaling and EndoMT contribute to atherosclerosis. To model this *in vitro*, mouse aortic
434 ECs (MAECs) from WT/ApoE$^{-/-}$ and EC-iCD45KO/ApoE$^{-/-}$ mice were isolated and treated
435 with tamoxifen, followed by stimulation with 100 μg/mL oxLDL to initiate EndoMT. Cell

436 mRNA was collected for quantitative RT-PCR assays to detect expression of the EndoMT
437 markers TGFβR2 and TGFβR3. MAECs with tamoxifen-induced CD45 deletions had reduced
438 $TGF\beta R_2$ (~64.26%; p = 0.0073) and $TGF\beta R_3$ (~59.04%; p = 0.0139) mRNA levels (**Figure 4J**
439 and **4K**). We confirmed an 84.52% (p<0.0001) reduction of CD45 mRNA expression in EC-
440 iCD45KO MAECs compared with the WT/ApoE$^{-/-}$ control group when treated with oxLDL
441 (100 μg/mL). Subsequent analyses showed reductions of MYH9 (~63.44%; p<0.0001),
442 Col1A1 (~58.26%; p = 0.0273), Twist (~53.15%; p = 0.0004) and Slug (~35.58%; p = 0.0003)
443 mRNA expression in EC-iCD45DKO MAECs compared to the control group. We also
444 observed an upregulation of approximately 1.75-fold (p = 0.0350) for FGFR2 mRNA levels in
445 MAECs from EC-iCD45DKO mice when compared to the ECs treated only with oxLDL.
446 These *in vitro* results confirm that loss of endothelial CD45 decreases EndoMT marker
447 expression and TGFβ signaling. CD45 deletion from MAECs also increases FGFR2 mRNA
448 expression. As discussed previously, increases in FGF receptor expression and KLF2 are
449 known to inhibit TGFβ signaling in ECs to attenuate EndoMT.

450 **Endothelial Loss of CD45 Prevents Inflammation and Atherosclerosis**

451 To substantiate our findings that the loss of CD45 expression can constrain the progression of
452 atherosclerosis, we performed histological staining on male and female ApoE$^{-/-}$ and EC-
453 iCD45KO/ApoE$^{-/-}$ mice fed a WD. We evaluated the aortic sinus and abdominal aorta as well
454 as performing *en face* preparations of the whole aorta. Whole mount *en face* aortas from ApoE^{-}
455 $^{/-}$ and EC-iCD45KO/ApoE$^{-/-}$ mice were stained with Oil Red O (**Figure 5A**, **B**: 8–13-week WD;
456 **Figure 5C**, **5D**: 10–13-week WD). We found that EC-iCD45KO/ApoE$^{-/-}$ mice fed an
457 atherosclerotic WD exhibited significant reductions in lesional area throughout the aorta
458 (~23.88%; ~8-13 week WD;~36.79%, 10-13 week WD) when compared with ApoE-null mice
459 that expressed CD45. Overall, these results indicate that loss of endothelial CD45 prevents
460 atherosclerosis progression.

461 To determine whether this phenomenon extends to regions of the vasculature beyond the aorta,
462 we assessed the aortic root and BCA from ApoE$^{-/-}$ and EC-iCD45KO/ApoE$^{-/-}$ mice fed a WD
463 for 16 weeks. Sections from these tissues were immunofluorescently-stained for both the
464 macrophage marker CD68 and α-SMA. We also created a tamoxifen-inducible endothelial-
465 specific lineage tracing system in the presence or absence of endothelial CD45 (**Figure S9A**).
466 Aortic root sections from ApoE$^{-/-}$/TdTomato and EC-iCD45KO/ApoE$^{-/-}$/TdTomato mice fed a
467 WD for 16 weeks were also used for immunofluorescence staining. We showed that α-SMA

468 expression was reduced in the aortic root endothelium in EC-iCD45KO/ApoE$^{-/-}$/TdTomato
469 mice compared to ApoE$^{-/-}$ mice (**Figure S9B**), which supports the contention that loss of
470 endothelial CD45 inhibits EndoMT.

471 Additional substantiation of this assertion comes from experiments demonstrating diminished
472 foam cell formation and α-SMA expression in arteries from CD45-deficient mice (**Figure 5E**
473 to **5G**). These studies revealed reductions in atherosclerotic lesion prevalence in aortic roots
474 (~25.39%; 12-week WD), BCAs (~28.28%; 16-week WD) and abdominal aortas (~40.05%;
475 16-week WD) in endothelial CD45-deficient mice (**Figure 5H** to **5M**) using H&E staining. We
476 also performed Oil Red O staining on aortic roots and BCAs to confirm the observed reductions
477 in atherosclerotic lesion burden as a result of CD45 loss (**Figure S10A** to **S10D**). CD45^{+}/VE-
478 Cadherin^{+}/α-SMA^{+} cells were significantly increased from 0.8 ± 1.0% in WT mice (n = 3) to
479 9.2 ± 0.7% in ApoE$^{-/-}$ WD-fed mice (n = 3) (p = 0.0003) compared to normal diet-fed ApoE$^{-/-}$
480 mice. The presence of α-SMA^{+} in ApoE$^{-/-}$ WD-fed mice indicates CD45^{+} ECs underwent
481 EndoMT within an aortic atherosclerotic lesion (**Figure S10E**). This finding is consistent with
482 the above cytometric analyses of total aortic cells for VE-Cadherin, FGFR1 and CD45
483 expression that showed a significant reduction in VE-Cadherin^{+}/FGFR1^{+} ECs in WD-fed
484 ApoE$^{-/-}$ mice compared to normal diet-fed ApoE$^{-/-}$ mice. It is also worth noting that all
485 immunofluorescence staining described above was performed alongside experimental controls
486 using serial sections stained with isotype-matched control IgGs (**Figure S11A to S11C**) to
487 ensure the validity of antibody staining. A graphical depiction of our findings (**Figure 6**)
488 highlights the novel role of CD45 in atherosclerosis progression through EndoMT regulation.

489 **DISCUSSION**

490 Our data show that deletion of CD45 from endothelial cells reduces atheroma burden in ApoE-
491 null mice fed a Western diet (WD). Our single-cell experiments further indicate that EC-
492 specific knock-out of CD45 moderates a novel sub-population of EndoMT cells, designated
493 EndoMT2. We present evidence that CD45 deficiency leads to decreases in TGFβR_2, TGFβR_3,
494 Twist, Slug, MYH9 and Col1a1 expression in MAECs pre-treated with oxLDL. In addition,
495 we unexpectedly discovered that the absence of endothelial CD45 led to the reduction of α-
496 smooth muscle actin and Col1a1, which are typical of EndoMT, in the aortic plaque. Finally,
497 we found endothelial CD45 deficiency increased KLF2 expression in the aortic plaque, a
498 transcription factor known to counter EndoMT, as well as augmenting FGFR2 expression.

499 Because the canonical hematopoietic marker CD45 is commonly used as a negative marker for
500 ECs, the existence of CD45-positive ECs may have been overlooked in previous studies despite
501 increasing evidence that indicates CD45-positive ECs are associated with certain pathological
502 conditions[44]. In a rat pulmonary arterial hypertension model, lung ECs were found to express
503 CD45 and endothelial function was verified by tubule formation in cocultures with lung
504 fibroblasts[2]. Protein tyrosine phosphatase receptor type C (CD45)-positive endothelium has
505 also been observed in the mitral valves of adult sheep 6 months after myocardial infarction
506 resulting in an EndoMT phenotype[4]. Moreover, the CD45 phosphatase inhibitor is reported to
507 block EndoMT activity in TGFβ1-treated ovine mitral valve ECs[4]. Taken together these studies
508 implicate endothelial CD45 in heart valve development and cardiovascular disease.

509 In this study, we discovered CD45-positive ECs in the aortic arches of patients with
510 atherosclerosis, which reinforces the notion that endothelial CD45 plays a vital role in human
511 cardiovascular disease (**Figure 1A and 1B**). Our results also reveal that loss of endothelial
512 CD45 results in a more favorable outcome in an established mouse model of atherosclerosis.
513 In the absence of endothelial CD45, ApoE-null mice fed a WD demonstrate reductions in
514 atherosclerotic lesion size in the aortic sinus, brachiocephalic artery (BCA), and abdominal
515 aorta. We also observed reductions in lesional area throughout the thoracic and abdominal aorta.
516 Overall, these findings plainly indicate that a lack of CD45 from the vascular endothelium
517 inhibits atherosclerosis progression in various arteries.

518 Although EndoMT contributes to atherosclerotic pathobiology and is associated with more
519 structurally complex plaques[15], the detailed molecular mechanisms by which CD45 drives
520 EndoMT and the therapeutic potential of manipulating CD45 expression in atherosclerosis

521 remains unknown. Our single-cell RNA-seq analyses provide an unbiased overview of how the
522 transcriptome changes in individual aortic cells[45]. Through single-cell clustering and cell type
523 annotation, we identified the four vascular cell types (**Figure 2A)**: ECs, VSMCs and two
524 distinct cell populations that we designated as EndoMT1 and EndoMT2. In EC-iCD45KO mice,
525 the EC population increases while VSMCs and the EndoMT1 and EndoMT2 populations
526 decrease, which indicates CD45 plays a role in determining vascular cell identity and function.

527 Analyses of the two EndoMT sub-populations showed that EC-specific CD45 deletion reduces
528 the number of cells in the EndoMT2 sub-population in atherosclerotic mice but had less impact
529 on the EndoMT1 sub-population. Cell identity gene analyses on these two sub-populations
530 showed their strong association with EndoMT-associated GO pathways such as TGFβ
531 signaling, mesenchymal development, and inflammatory signals (**Figure 2K)**. Moreover, the
532 RNA velocity as well as trajectory and cell-cell communication analyses revealed that the
533 EndoMT process is prevalent in WT/ApoE$^{-/-}$ (**Figure 3C to 3D**) and driven by CD45 and
534 TGFβ1 genes (**Figure 3F**). Deletion of CD45 in ECs appears to modulate EndoMT processes
535 by promoting a transition toward MendoT; although, the veracity of this evidence will need to
536 be investigated in future studies using single-cell lineage tracing techniques in mouse models,
537 such as DARLIN and CARLIN[46].

538 As noted above, CD45 is not normally expressed in ECs and the details of how it might regulate
539 normal or partial EndoMT remains an open question. This process might be triggered by cross-
540 talk signaling regulatory mechanisms that limit progression through the EndoMT. ECs may
541 undergo progressive transition to a mesenchymal phenotype through intermediate cell states
542 (*i.e.*, partial EndoMT) that enable temporary and reversible adoption of a hybrid endothelial-
543 mesenchymal cell state. It is known that during the early stages of neointima formation, ECs
544 transiently express CD45 accompanied by a host of EndoMT markers[47]. Yamashiro and
545 colleagues also showed that CD31 and α-SMA were expressed in the developing neointima in
546 a carotid artery ligation model[47].

547 In this study, human aortic ECs were treated with cobalt chloride ($CoCl_2$), a hypoxia-inducible
548 factor (HIF) activator, which resulted in upregulation of CD45 expression[47]. Inhibition of
549 CD45 PTPase activity caused a similar elongated morphology to $CoCl_2$ treatment; however,
550 the cells treated with $CoCl_2$ and CD45 PTPase inhibitor showed a significant decrease in VE-
551 Cadherin expression and prominent actin stress fibers. These results suggest that HIF-induced
552 CD45 expression is normally required for the retention of EC fate and cell–cell junctions, and

553 that CD45-positive partial EndoMT contributes to neointima formation and vascular
554 remodeling[47]. While these findings are certainly novel, it is unclear if CD45-positive partial
555 EndoMT is beneficial and more work needs to be done before a mechanism is established.

556 Nevertheless, our single-cell results comport with these observations as they identified a unique
557 CD45-dependent EndoMT population in the aortic endothelium (EndoMT2 cells) that is
558 seemingly involved in the progressive transition to intermediate mesenchymal cell states in
559 ApoE$^{-/-}$ mice when compared to EC-iCD45KO/ApoE$^{-/-}$ mice fed a WD for 16 weeks. In
560 addition, we observed a reduction of TGFβR2 and TGFβ1 expression using single-cell analysis
561 of the EndoMT2 sub-population from the endothelial CD45-deficient atherosclerotic mice
562 opposed to WT/ApoE$^{-/-}$ mice on a WD for 16 weeks. These observations indicate that
563 endothelial CD45 also mediates partial EndoMT during advanced atherosclerosis[44].

564 Previous studies showed that FGFR2 mutations can affect cell responses to TGFβ stimulation
565 via the ERK pathway, which is, at least in part, because of an altered balance between FGF and
566 TGFβ signaling[48]. Consequently, maintaining FGFR2 expression can antagonize TGFβ to
567 restrict EndoMT progression within atherosclerotic lesions. Our study demonstrates that CD45
568 expression negatively correlates with FGFR2 mRNA expression in MAECs to affect FGFR2
569 signaling, implying that CD45 inhibition can enhance FGFR2 signaling[48]. As FGFR signaling
570 can obstruct TGFβR-dependent signaling, this may attenuate EndoMT during atherosclerosis.

571 In line with this hypothesis, it has been reported that FGFR2 overexpression in ECs increases
572 viability, suppresses apoptosis and oxidative stress, and improves endothelial function[49]. In the
573 previously mentioned study on neointima formation[47], CD45 was detected in cells undergoing
574 EndoMT, and activation of TGFβ signaling was evident in the early neointimal cells as was the
575 expression of Snail, Slug and pSmad2/3[47]. This corresponds with our data where we observed
576 less TGFβR2 and TGFβR3 expression in CD45-deficient MAECs when compared with WT
577 cells. Our findings also show a reduction in the expression of Slug, Twist, MYH9 and Col1a1
578 in EC-iCD45KO ECs opposed to WT MAECs treated with oxLDL[47]. These findings provide
579 strong evidence that CD45-regulated EndoMT is indispensable for FGFR2 and TGF*β* signal
580 transduction (**Figure 6)**. In addition, preserving KLF2 expression suppresses EndoMT and
581 mitigates endothelial dysfunction during atherosclerosis[50], which is also consistent with our
582 findings.

583 In summary, we report the first evidence that in a mouse model of atherosclerosis, the absence
584 of endothelial CD45 leads to reduced lesion development, foam cell infiltration and expression

585 of adhesion molecules in atherosclerosis. Single-cell experiments identified a unique, CD45-
586 dependent EndoMT population in the aortic endothelium (EndoMT2 cells) that mediates partial
587 EndoMT in atherosclerosis[44]. In addition, endothelial CD45 deficiency led to reduced
588 expression of α-SMA and Col1a1, while increasing FGFR2 expression that results in reduced
589 EndoMT and atherosclerotic lesion progression. These findings highlight the potential for
590 therapeutically-targeting endothelial CD45 for the treatment of atherosclerosis, which is the
591 leading cause of death in the United States.

592 **Author Contributions**

593 Q.P. and H.C. conceived the project. K.A. performed all single-cell data analysis and wrote the
594 original draft of the single-cell data analysis. Q.P. wrote the original draft, performed most of
595 the experiments. Y.W.L. assisted with most of the study. Q.P. and Y.W.L. participated in the
596 experiment design for IF staining and data analysis. B.Z. performed single-cell cDNA library
597 construction. K.C. assisted with *en face* Oil Red O staining and performed a lipid panel test.
598 B.S. assisted with parts of the study, including the studies of MAECs. M.V.M. performed most
599 of the blood counts and lipid panel tests. Q.P. and J.W-S. performed most of the genotype
600 work. J.W-S. assisted with all the genotype work and flow cytometry analysis. S. W. performed
601 the remaining genotype work. Q.P., K.A., J. W-S., K.C., J.B. and H.C. contributed to in-depth
602 discussions of the results. Q.P., K.A., Y.W.L., B.Z., B.S., K.C., J.W-S., S.W., D.B.C., M.A.,
603 D-Z.W., K.F.C., J.B., and H.C. reviewed and edited the manuscript.

604 **Sources of Funding**

605 This project was supported by NIH R01HL146134 (H.C. and D.W.), an American Heart
606 Association Transformational Project Award (H.C.), an American Heart Association
607 Postdoctoral fellowship 23POST1021226 (P.Q.), and, in part, by NIH R01HL156362 (H.C.),
608 R01HL158097 (H.C.), R01HL162367 (H.C.), R01HL174928 (H.C., D.W., and K.F.C.)
609 K99HL171947 (K.F.C.), R01GM125632 (K.F.C.), and R01GM138407 (K.F.C.).

610 **Data Availability**

611 The authors declare that all supporting data are available within the article and its Supplemental
612 Material. Additional methods or data related to this study are available from the corresponding
613 authors upon reasonable request. The scRNA-seq data generated in this study were deposited
614 into the GEO database with the accession number GSE313399.

615 **FIGURE LEGENDS**

616 **Figure 1. Endothelial CD45-dependent EndoMT during atherosclerosis. A**,
617 Immunofluorescence staining of the aortic arch section from atherosclerosis patients for CD45
618 (green) and VE-Cadherin (red) (Scale bar = 10 μm). **B**, Single-cell expression profiles of CD45
619 and endothelial functional genes in CD31 expressing cells of human healthy control and
620 atherosclerosis patients. **C**, Aortas from ApoE$^{-/-}$ mice fed a normal diet versus WD — lesions
621 are apparent in ApoE$^{-/-}$ WD-fed aortas (Scale bar = 10 μm). **D**, Representative flow cytometry
622 analysis of ECs labeled with anti-VE-cadherin-FITC, anti-CD45-CF647, and anti-FGFR1-PE.
623 Circles (n = 3) highlight increased FGFR1-negative ECs in ApoE$^{-/-}$ WD aortas. Squares (n =
624 5) indicate increased CD45 ECs in WD-fed aortas from ApoE$^{-/-}$ mice. **E**, Flow cytometric
625 analysis of FGFR1+ EC from ApoE$^{-/-}$ normal diet (black circles, n = 3) and ApoE$^{-/-}$ WD (red
626 squares, n = 5) mice. FGFR1+ ECs are decreased (p = 0.0324) in ApoE$^{-/-}$ WD-fed mice aortas.
627 **F**, Diagram showing the timeline for the deletion induced by tamoxifen injections. **G**,
628 Immunostaining of aortic root sections from WT/ApoE$^{-/-}$ and EC-iCD45KO/ApoE$^{-/-}$ mice fed
629 with western diet (WD) for 12 weeks for CD45 (green) and CD31 (red). **H**, Quantification of
630 CD31+/CD45+ cells WT/ApoE$^{-/-}$ and EC-iCD45KO/ApoE$^{-/-}$ mice fed with western diet (WD)
631 for 12 weeks. **I**, Aortas from WT/ApoE$^{-/-}$ mice versus EC-iCD45KO/ApoE$^{-/-}$ mice fed with
632 western diet (WD) for 16 weeks. **J**, *En face* aortas from WT/ApoE$^{-/-}$ and ECiCD45KO/ApoE^{-}
633 $^{/-}$ female mice stained with Oil Red O (16-week WD) (Scale bar = 200 μm). **K,** Quantification
634 of lesion area in the aortas.

635 **Figure 2**. **Endothelial cell-specific deletion of CD45 rewires vascular cell identity in**
636 **WT/ApoE$^{-/-}$ and EC-iCD45KO/ApoE$^{-/-}$ mice. A**, Five vascular cell types were identified
637 using scRNA-seq data from WT/ApoE$^{-/-}$ and EC-iCD45KO/ApoE$^{-/-}$ mice. **B**, Bar graph
638 depicting the percentage of each cell population in aortas from WT/ApoE$^{-/-}$ and EC-
639 iCD45KO/ApoE$^{-/-}$ mice. **C-H**, Expression levels of endothelial (C, F), VSMC (D, G) functional
640 genes and EndoMT markers (E, H), shown by violin plot, in EndoMT1 (C-E) and EndoMT2
641 (F-H) cells between WT/ApoE$^{-/-}$ and EC-iCD45KO/ApoE$^{-/-}$ mice. **I**, Scatter plot showing the
642 Pearson correlation between cell identity gene (CIG) scores of EndoMT1 and EndoMT2 cells
643 in WT/ApoE$^{-/-}$ (left) and EC-iCD45KO/ApoE$^{-/-}$ (right) mice. **J**, Venn diagram depicting shared
644 and unique cell identity genes identified by the SCIG tool in EndoMT1 and EndoMT2 cells of
645 WT/ApoE$^{-/-}$ mice. **K**, Pathway analysis of shared CIGs EndoMT genes between EndoMT1 and
646 2 cells strongly implicated in EndoMT processes. **L**, Pearson correlation of cell identity gene

647 scores for each vascular cell type between WT/ApoE$^{-/-}$ and EC-iCD45KO/ApoE$^{-/-}$ mice. **M**,
648 Gene concept diagrams illustrate Gene Ontology (GO) pathway enrichment of unique cell-
649 identity genes identified in EndoMT2 cells. In WT/ApoE$^{-/-}$ mice (left), enriched pathways are
650 primarily associated with inflammatory, cytokine-mediated, and muscle-related functional
651 processes. In EC-iCD45KO/ApoE$^{-/-}$ mice (right), enriched pathways are predominantly related
652 to endothelial cell function and angiogenesis.

653 **Figure 3. Role of CD45 in EndoMT using single-cell dynamics and cell-cell**
654 **communication analyses. A**, RNA velocity analysis shows the transition of endothelial cells
655 (ECs) to vascular smooth muscle cells (VSMCs) through EndoMT cells in WT/ApoE$^{-/-}$ mice
656 (left), a process that is absent in EC-iCD45KO/ApoE$^{-/-}$ mice. Instead, a mesenchymal-to-
657 endothelial transition (MEndoT) process is observed (right). Solid black outlines indicate the
658 EndoMT trajectory, while dotted outlines indicate the MEndoT trajectory. **B**, Monocle3
659 trajectory inference analysis comparing WT/ApoE$^{-/-}$ and EC-iCD45KO/ApoE$^{-/-}$ mice. **C**, Gene
660 expression changes associated with the EndoMT and MendoT trajectories in WT/ApoE$^{-/-}$ and
661 EC-iCD45KO/ApoE$^{-/-}$ mice, respectively. **D**, Boxplots showing the ranking of vascular cell
662 types based on their pseudotime in WT/ApoE$^{-/-}$ (left) and EC-iCD45KO/ApoE$^{-/-}$ (right) mice.
663 **E**, Potential ligands identified in sender cells of WT/ApoE$^{-/-}$ and EC-iCD45KO/ApoE$^{-/-}$ mice.
664 **F-G**, Chord diagrams illustrating potential ligands and their regulation of target genes in
665 receiver ECs of WT/ApoE$^{-/-}$ mice (F) and CD45-deletion mice (G). **H-I**, Expression profiles
666 of identified target genes in receiver ECs of WT/ApoE$^{-/-}$ mice (H) and CD45-deletion mice (I)

667 **Figure 4. Endothelial CD45-deficiency inhibits EndoMT by reducing TGFβ signaling**
668 **while upregulating FGFR2 expression during atherosclerosis. A**, *En face* immunostaining
669 of the thoracic aorta was performed with antibodies to CD45, VE-Cadherin, and CD31; DAPI
670 staining shown to visualize nuclei (Scale bars = 50 μm). **B**, Enlarged images of immunostaining
671 for CD45 and CD31 and from Figure **4A** (Scale bars = 10 μm). **C**, Quantification for
672 colocalization of VE-Cadherin and CD45. **D**, *En face* immunostaining of the thoracic aorta was
673 performed with antibodies to ICAM-1, VE-Cadherin, and CD31; DAPI staining shown to
674 visualize nuclei (Scale bars = 50 μm). **E**, Enlarged images of immunostaining for ICAM-1 and
675 CD31 from panel D (Scale bars = 20 μm). **F**, Quantification of colocalized VE-Cadherin and
676 ICAM-1 in the thoracic aorta. **G**, Aortic root sections from WT/ApoE$^{-/-}$ and EC-iCD45KO
677 ApoE$^{-/-}$ mice were co-stained with the Col1a1 and VE-Cadherin. **H**, Enlarged images of
678 immunostaining for Col1a1and VE-Cadherin from Figure 4 **G** (Scale bars = 20 μm). **I**,

679 Quantification of colocalized Col1a1 and VE-Cadherin in the aortic root. **J**, MAECs isolated
680 from of WT/ApoE$^{-/-}$ and EC-iCD45KO/ApoE$^{-/-}$ mice were treated with 5 μmol/L tamoxifen for
681 3 days, followed by treatment with 100 μg/mL oxidized low-density lipoprotein, and then lysed
682 for quantitative polymerase chain reaction to detect endothelial-to-mesenchymal transition
683 (EndoMT) markers (n = 3). Reductions in expression of Twist and Slug, genes associated with
684 the EndoMT process, were seen in CD45 KO MAECs. MYH9 and Col1a1 were also
685 significantly reduced, while FGFR2 was significantly upregulated. **K**, TGFβR2 and TGFβR3
686 were significantly reduced in endothelial CD45 KO MAEC.

687 **Figure 5. Endothelial CD45 deletion reduces atherosclerosis in ApoE$^{-/-}$ mice. A-D**, *En*
688 *face* aorta preparations from WT/ApoE$^{-/-}$ and EC-iCD45KO /ApoE$^{-/-}$ male (A, 8–13-week WD)
689 and female (C, 10-13 week WD) mice stained with Oil Red O. Quantifications for *en face* Oil
690 Red O staining in male (B) and female mice (D) (Scale bar = 200 μm). **E-G**, Aortic root sections
691 from WT/ApoE$^{-/-}$ and EC-iCD45KO ApoE$^{-/-}$ mice were stained with antibodies against the
692 macrophage marker CD68 and α-SMA (E, Scale bar = 200 μm). Quantifications for CD68 (F)
693 and α-SMA (G) staining. **H-M**, Hematoxylin and eosin (H&E) staining of the aortic root (H);
694 aortic aneurysm sections (J); and brachiocephalic artery (L). Quantifications for H&E staining
695 in the aortic root (I), aortic aneurysm sections (K), and brachiocephalic artery (M) (Scale bars
696 = 10 μm).

697 **Figure 6. Loss of endothelial CD45 reduces EndoMT and atherosclerosis in WT/ApoE^{-}**
698 **$^{/-}$ mice.** EndoMT can be induced by several factors including TGFβ signaling, inflammatory
699 cytokines, and expression of the protein tyrosine phosphatase CD45. During this process,
700 CD45-positive (termed as 'partial EndoMT') cells contribute to neointima formation and
701 vascular wall remodeling. Twist, MYH9, Col1a1 expression has been indicated to be reduced
702 in EC-iCD45KO cells compared to that in the control MAECs. Expression of FGFR2 has been
703 raised in EC-iCD45KO cells compared to that in the control mice. Additionally, it has been
704 reported that ERK pathway levels and p-Smad2 expression were higher in the CD45-positive
705 cells than in the cells from control mice.

REFERENCES

1. Justement LB. The role of CD45 in signal transduction. *Adv Immunol*. 1997;66:1-65. doi: 10.1016/s0065-2776(08)60595-7
2. Hong J, Wong B, Huynh C, Tang B, Ruffenach G, Li M, Umar S, Yang X, Eghbali M. Tm4sf1-marked Endothelial Subpopulation Is Dysregulated in Pulmonary Arterial Hypertension. *Am J Respir Cell Mol Biol*. 2023;68:381-394. doi: 10.1165/rcmb.2022-0020OC
3. Nasim S, Wylie-Sears J, Gao X, Peng Q, Zhu B, Chen K, Chen H, Bischoff J. CD45 Is Sufficient to Initiate Endothelial-to-Mesenchymal Transition in Human Endothelial Cells-Brief Report. *Arterioscler Thromb Vasc Biol*. 2023;43:e124-e131. doi: 10.1161/ATVBAHA.122.318172
4. Bischoff J, Casanovas G, Wylie-Sears J, Kim DH, Bartko PE, Guerrero JL, Dal-Bianco JP, Beaudoin J, Garcia ML, Sullivan SM, et al. CD45 Expression in Mitral Valve Endothelial Cells After Myocardial Infarction. *Circ Res*. 2016;119:1215-1225. doi: 10.1161/CIRCRESAHA.116.309598
5. Martin SS, Aday AW, Almarzooq ZI, Anderson CAM, Arora P, Avery CL, Baker-Smith CM, Barone Gibbs B, Beaton AZ, Boehme AK, et al. 2024 Heart Disease and Stroke Statistics: A Report of US and Global Data From the American Heart Association. *Circulation*. 2024;149:e347-e913. doi: 10.1161/CIR.0000000000001209
6. Khatana C, Saini NK, Chakrabarti S, Saini V, Sharma A, Saini RV, Saini AK. Mechanistic Insights into the Oxidized Low-Density Lipoprotein-Induced Atherosclerosis. *Oxid Med Cell Longev*. 2020;2020:5245308. doi: 10.1155/2020/5245308
7. Lorey MB, Oorni K, Kovanen PT. Modified Lipoproteins Induce Arterial Wall Inflammation During Atherogenesis. *Frontiers in cardiovascular medicine*. 2022;9:841545. doi: 10.3389/fcvm.2022.841545
8. Gialeli C, Shami A, Goncalves I. Extracellular matrix: paving the way to the newest trends in atherosclerosis. *Curr Opin Lipidol*. 2021;32:277-285. doi: 10.1097/MOL.0000000000000775
9. Gan AM, Pirvulescu MM, Stan D, Simion V, Calin M, Manduteanu I, Butoi E. Monocytes and smooth muscle cells cross-talk activates STAT3 and induces resistin and reactive oxygen species production [corrected]. *J Cell Biochem*. 2013;114:2273-2283. doi: 10.1002/jcb.24571
10. Moore KJ, Tabas I. Macrophages in the pathogenesis of atherosclerosis. *Cell*. 2011;145:341-355. doi: 10.1016/j.cell.2011.04.005
11. Gimbrone MA, Jr., Garcia-Cardena G. Endothelial Cell Dysfunction and the Pathobiology of Atherosclerosis. *Circ Res*. 2016;118:620-636. doi: 10.1161/CIRCRESAHA.115.306301
12. Kovacic JC, Dimmeler S, Harvey RP, Finkel T, Aikawa E, Krenning G, Baker AH. Endothelial to Mesenchymal Transition in Cardiovascular Disease: JACC State-of-the-Art Review. *J Am Coll Cardiol*. 2019;73:190-209. doi: 10.1016/j.jacc.2018.09.089
13. Peng Q, Shan D, Cui K, Li K, Zhu B, Wu H, Wang B, Wong S, Norton V, Dong Y, et al. The Role of Endothelial-to-Mesenchymal Transition in Cardiovascular Disease. *Cells*. 2022;11. doi: 10.3390/cells11111834
14. Piera-Velazquez S, Jimenez SA. Endothelial to Mesenchymal Transition: Role in Physiology and in the Pathogenesis of Human Diseases. *Physiol Rev*. 2019;99:1281-1324. doi: 10.1152/physrev.00021.2018
15. Evrard SM, Lecce L, Michelis KC, Nomura-Kitabayashi A, Pandey G, Purushothaman KR, d'Escamard V, Li JR, Hadri L, Fujitani K, et al. Endothelial to mesenchymal

transition is common in atherosclerotic lesions and is associated with plaque instability. *Nat Commun*. 2016;7:11853. doi: 10.1038/ncomms11853
16. Chen PY, Qin L, Baeyens N, Li G, Afolabi T, Budatha M, Tellides G, Schwartz MA, Simons M. Endothelial-to-mesenchymal transition drives atherosclerosis progression. *J Clin Invest*. 2015;125:4514-4528. doi: 10.1172/JCI82719
17. Chen PY, Qin L, Li G, Wang Z, Dahlman JE, Malagon-Lopez J, Gujja S, Cilfone NA, Kauffman KJ, Sun L, et al. Endothelial TGF-beta signalling drives vascular inflammation and atherosclerosis. *Nat Metab*. 2019;1:912-926. doi: 10.1038/s42255-019-0102-3
18. Pickett JR, Wu Y, Zacchi LF, Ta HT. Targeting endothelial vascular cell adhesion molecule-1 in atherosclerosis: drug discovery and development of vascular cell adhesion molecule-1-directed novel therapeutics. *Cardiovasc Res*. 2023;119:2278-2293. doi: 10.1093/cvr/cvad130
19. Yang X, Liaw L, Prudovsky I, Brooks PC, Vary C, Oxburgh L, Friesel R. Fibroblast growth factor signaling in the vasculature. *Curr Atheroscler Rep*. 2015;17:509. doi: 10.1007/s11883-015-0509-6
20. Chen PY, Simons M. Fibroblast growth factor-transforming growth factor beta dialogues, endothelial cell to mesenchymal transition, and atherosclerosis. *Curr Opin Lipidol*. 2018;29:397-403. doi: 10.1097/MOL.0000000000000542
21. Lingrel JB, Pilcher-Roberts R, Basford JE, Manoharan P, Neumann J, Konaniah ES, Srinivasan R, Bogdanov VY, Hui DY. Myeloid-specific Kruppel-like factor 2 inactivation increases macrophage and neutrophil adhesion and promotes atherosclerosis. *Circ Res*. 2012;110:1294-1302. doi: 10.1161/CIRCRESAHA.112.267310
22. Matsunaga S, Okigaki M, Takeda M, Matsui A, Honsho S, Katsume A, Kishita E, Che J, Kurihara T, Adachi Y, et al. Endothelium-targeted overexpression of constitutively active FGF receptor induces cardioprotection in mice myocardial infarction. *J Mol Cell Cardiol*. 2009;46:663-673. doi: 10.1016/j.yjmcc.2009.01.015
23. Dong Y, Wang B, Du M, Zhu B, Cui K, Li K, Yuan K, Cowan DB, Bhattacharjee S, Wong S, et al. Targeting Epsins to Inhibit Fibroblast Growth Factor Signaling While Potentiating Transforming Growth Factor-beta Signaling Constrains Endothelial-to-Mesenchymal Transition in Atherosclerosis. *Circulation*. 2023;147:669-685. doi: 10.1161/CIRCULATIONAHA.122.063075
24. Dong Y, Lee Y, Cui K, He M, Wang B, Bhattacharjee S, Zhu B, Yago T, Zhang K, Deng L, et al. Epsin-mediated degradation of IP3R1 fuels atherosclerosis. *Nat Commun*. 2020;11:3984. doi: 10.1038/s41467-020-17848-4
25. Wang JM, Chen AF, Zhang K. Isolation and Primary Culture of Mouse Aortic Endothelial Cells. *J Vis Exp*. 2016. doi: 10.3791/52965
26. Zheng GX, Terry JM, Belgrader P, Ryvkin P, Bent ZW, Wilson R, Ziraldo SB, Wheeler TD, McDermott GP, Zhu J, et al. Massively parallel digital transcriptional profiling of single cells. *Nat Commun*. 2017;8:14049. doi: 10.1038/ncomms14049
27. Hao Y, Stuart T, Kowalski MH, Choudhary S, Hoffman P, Hartman A, Srivastava A, Molla G, Madad S, Fernandez-Granda C, et al. Dictionary learning for integrative, multimodal and scalable single-cell analysis. *Nat Biotechnol*. 2024;42:293-304. doi: 10.1038/s41587-023-01767-y
28. McGinnis CS, Murrow LM, Gartner ZJ. DoubletFinder: Doublet Detection in Single-Cell RNA Sequencing Data Using Artificial Nearest Neighbors. *Cell Syst*. 2019;8:329-337 e324. doi: 10.1016/j.cels.2019.03.003

29. Franzen O, Gan LM, Bjorkegren JLM. PanglaoDB: a web server for exploration of mouse and human single-cell RNA sequencing data. *Database (Oxford)*. 2019;2019. doi: 10.1093/database/baz046
30. Hu C, Li T, Xu Y, Zhang X, Li F, Bai J, Chen J, Jiang W, Yang K, Ou Q, et al. CellMarker 2.0: an updated database of manually curated cell markers in human/mouse and web tools based on scRNA-seq data. *Nucleic Acids Res*. 2023;51:D870-D876. doi: 10.1093/nar/gkac947
31. Yu G, Wang LG, Han Y, He QY. clusterProfiler: an R package for comparing biological themes among gene clusters. *OMICS*. 2012;16:284-287. doi: 10.1089/omi.2011.0118
32. Arulsamy K, Xia B, Yu Y, Chen H, Pu WT, Zhang L, Chen K. SCIG: Machine learning uncovers cell identity genes in single cells by genetic sequence codes. *Nucleic Acids Res*. 2025;53. doi: 10.1093/nar/gkaf431
33. Wirka RC, Wagh D, Paik DT, Pjanic M, Nguyen T, Miller CL, Kundu R, Nagao M, Coller J, Koyano TK, et al. Atheroprotective roles of smooth muscle cell phenotypic modulation and the TCF21 disease gene as revealed by single-cell analysis. *Nat Med*. 2019;25:1280-1289. doi: 10.1038/s41591-019-0512-5
34. Hu Z, Liu W, Hua X, Chen X, Chang Y, Hu Y, Xu Z, Song J. Single-Cell Transcriptomic Atlas of Different Human Cardiac Arteries Identifies Cell Types Associated With Vascular Physiology. *Arterioscler Thromb Vasc Biol*. 2021;41:1408-1427. doi: 10.1161/ATVBAHA.120.315373
35. Bergen V, Lange M, Peidli S, Wolf FA, Theis FJ. Generalizing RNA velocity to transient cell states through dynamical modeling. *Nat Biotechnol*. 2020;38:1408-1414. doi: 10.1038/s41587-020-0591-3
36. Qiu X, Hill A, Packer J, Lin D, Ma YA, Trapnell C. Single-cell mRNA quantification and differential analysis with Census. *Nat Methods*. 2017;14:309-315. doi: 10.1038/nmeth.4150
37. Gu Z. Complex heatmap visualization. *Imeta*. 2022;1:e43. doi: 10.1002/imt2.43
38. Browaeys R, Saelens W, Saeys Y. NicheNet: modeling intercellular communication by linking ligands to target genes. *Nat Methods*. 2020;17:159-162. doi: 10.1038/s41592-019-0667-5
39. Cui K, Gao X, Wang B, Wu H, Arulsamy K, Dong Y, Xiao Y, Jiang X, Malovichko MV, Li K, et al. Epsin Nanotherapy Regulates Cholesterol Transport to Fortify Atheroma Regression. *Circ Res*. 2023;132:e22-e42. doi: 10.1161/CIRCRESAHA.122.321723
40. Pan H, Xue C, Auerbach BJ, Fan J, Bashore AC, Cui J, Yang DY, Trignano SB, Liu W, Shi J, et al. Single-Cell Genomics Reveals a Novel Cell State During Smooth Muscle Cell Phenotypic Switching and Potential Therapeutic Targets for Atherosclerosis in Mouse and Human. *Circulation*. 2020;142:2060-2075. doi: 10.1161/CIRCULATIONAHA.120.048378
41. Lu YW, Martino N, Gerlach BD, Lamar JM, Vincent PA, Adam AP, Schwarz JJ. MEF2 (Myocyte Enhancer Factor 2) Is Essential for Endothelial Homeostasis and the Atheroprotective Gene Expression Program. *Arterioscler Thromb Vasc Biol*. 2021;41:1105-1123. doi: 10.1161/ATVBAHA.120.314978
42. Ganger MT, Dietz GD, Ewing SJ. A common base method for analysis of qPCR data and the application of simple blocking in qPCR experiments. *BMC Bioinformatics*. 2017;18:534. doi: 10.1186/s12859-017-1949-5
43. Arulsamy K, Cui K, Zhu B, Wang B, Eisa-Beygi S, Voronova A, Gao X, Gupta K, Zhang L, Chen K, et al. Single-Cell Analysis Reveals a Critical Role for Macrophage

Epsins in Regulating the Origin of Foam Cells in Atherosclerosis. *Arterioscler Thromb Vasc Biol*. 2025;45:e523-e543. doi: 10.1161/ATVBAHA.125.323288
44. Alvandi Z, Bischoff J. Endothelial-Mesenchymal Transition in Cardiovascular Disease. *Arterioscler Thromb Vasc Biol*. 2021;41:2357-2369. doi: 10.1161/ATVBAHA.121.313788
45. Li Y, Ren P, Dawson A, Vasquez HG, Ageedi W, Zhang C, Luo W, Chen R, Li Y, Kim S, et al. Single-Cell Transcriptome Analysis Reveals Dynamic Cell Populations and Differential Gene Expression Patterns in Control and Aneurysmal Human Aortic Tissue. *Circulation*. 2020;142:1374-1388. doi: 10.1161/CIRCULATIONAHA.120.046528
46. Zhang X, Huang Y, Yang Y, Wang QE, Li L. Advancements in prospective single-cell lineage barcoding and their applications in research. *Genome Res*. 2024;34:2147-2162. doi: 10.1101/gr.278944.124
47. Yamashiro Y, Ramirez K, Nagayama K, Hattori N, Liu YY, Matsunaga S, Tomita S, Kubota Y, Yanagisawa H. Partial endothelial-to-mesenchymal transition mediated by HIF-induced CD45 in neointima formation upon carotid artery ligation. *Cardiovasc Res*. 2023;119:1606-1618. doi: 10.1093/cvr/cvac190
48. Lee KM, Santos-Ruiz L, Ferretti P. A single-point mutation in FGFR2 affects cell cycle and Tgfbeta signalling in osteoblasts. *Biochimica et biophysica acta*. 2010;1802:347-355. doi: 10.1016/j.bbadis.2009.11.006
49. Jiao K, Su P, Li Y. FGFR2 modulates the Akt/Nrf2/ARE signaling pathway to improve angiotensin II-induced hypertension-related endothelial dysfunction. *Clin Exp Hypertens*. 2023;45:2208777. doi: 10.1080/10641963.2023.2208777
50. Cho DI, Ahn JH, Kang BG, Hwang I, Cho HH, Jun JH, Yoo J, Cho M, Yoo SJ, Kim HS, et al. ANGPTL4 Prevents Atherosclerosis by Preserving KLF2 to Suppress EndMT and Mitigates Endothelial Dysfunction. *Arterioscler Thromb Vasc Biol*. 2025;45:1742-1761. doi: 10.1161/ATVBAHA.125.322700

Figure 1

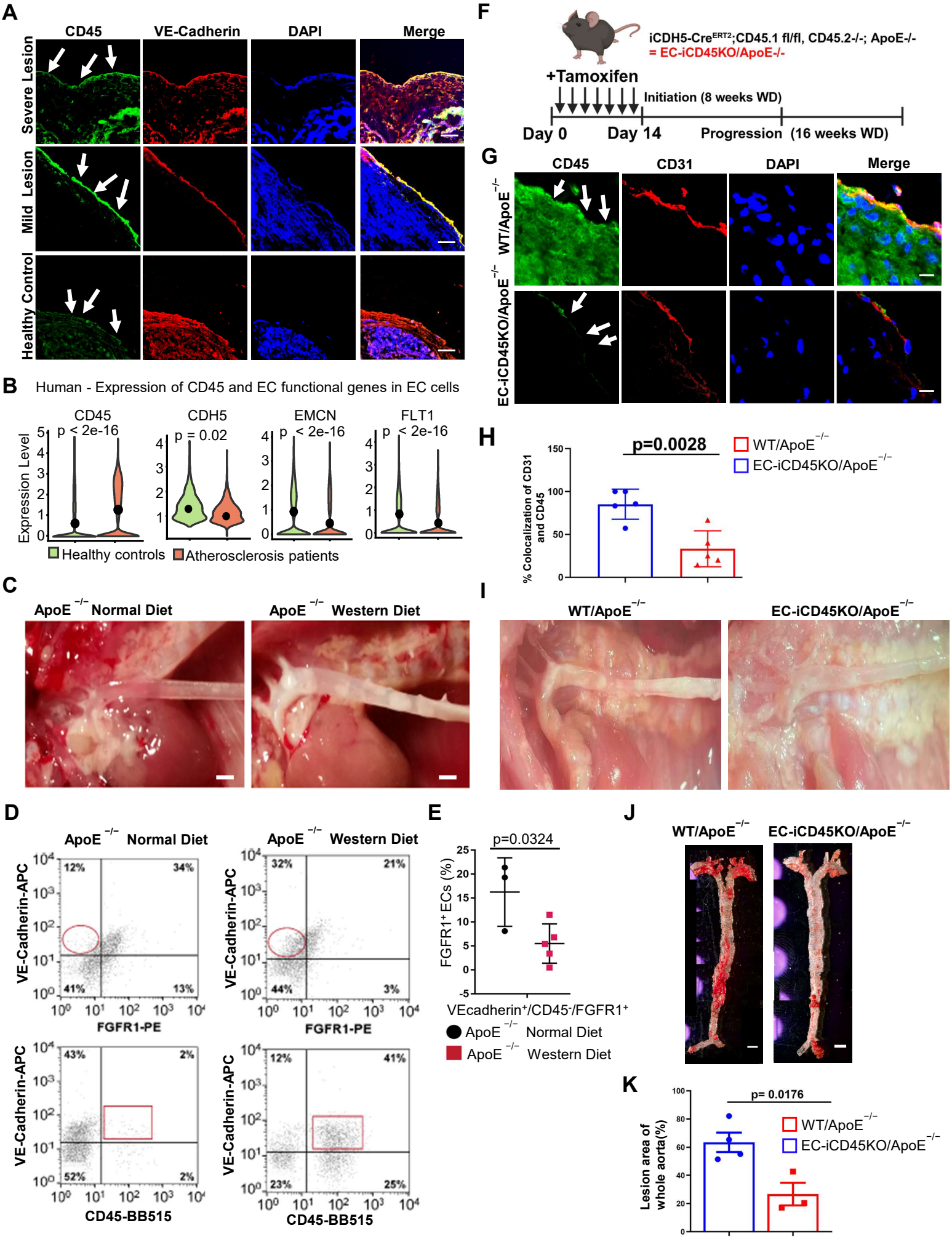
A
CD45
VE-Cadherin
DAPI
Merge
Severe Lesion
Mild Lesion
Healthy Control
B
Human - Expression of CD45 and EC functional genes in EC cells
CD45
p < 2e-16
CDH5
p = 0.02
EMCN
p < 2e-16
FLT1
p < 2e-16
Expression Level
Healthy controls
Atherosclerosis patients
C
ApoE −/− Normal Diet
ApoE −/− Western Diet
D
ApoE −/− Normal Diet
ApoE −/− Western Diet
VE-Cadherin-APC
FGFR1-PE
CD45-BB515
12%
34%
41%
13%
32%
21%
44%
3%
43%
2%
52%
2%
12%
41%
23%
25%
E
p=0.0324
FGFR1+ ECs (%)
VEcadherin+/CD45-/FGFR1+
ApoE −/− Normal Diet
ApoE −/− Western Diet
F
iCDH5-CreERT2;CD45.1 fl/fl, CD45.2-/-; ApoE-/-
= EC-iCD45KO/ApoE-/-
+Tamoxifen
Initiation (8 weeks WD)
Day 0
Day 14
Progression (16 weeks WD)
G
CD45
CD31
DAPI
Merge
WT/ApoE−/−
EC-iCD45KO/ApoE−/−
H
p=0.0028
WT/ApoE−/−
EC-iCD45KO/ApoE−/−
% Colocalization of CD31 and CD45
I
WT/ApoE−/−
EC-iCD45KO/ApoE−/−
J
WT/ApoE−/−
EC-iCD45KO/ApoE−/−
K
p= 0.0176
WT/ApoE−/−
EC-iCD45KO/ApoE−/−
Lesion area of whole aorta(%)

Figure 2

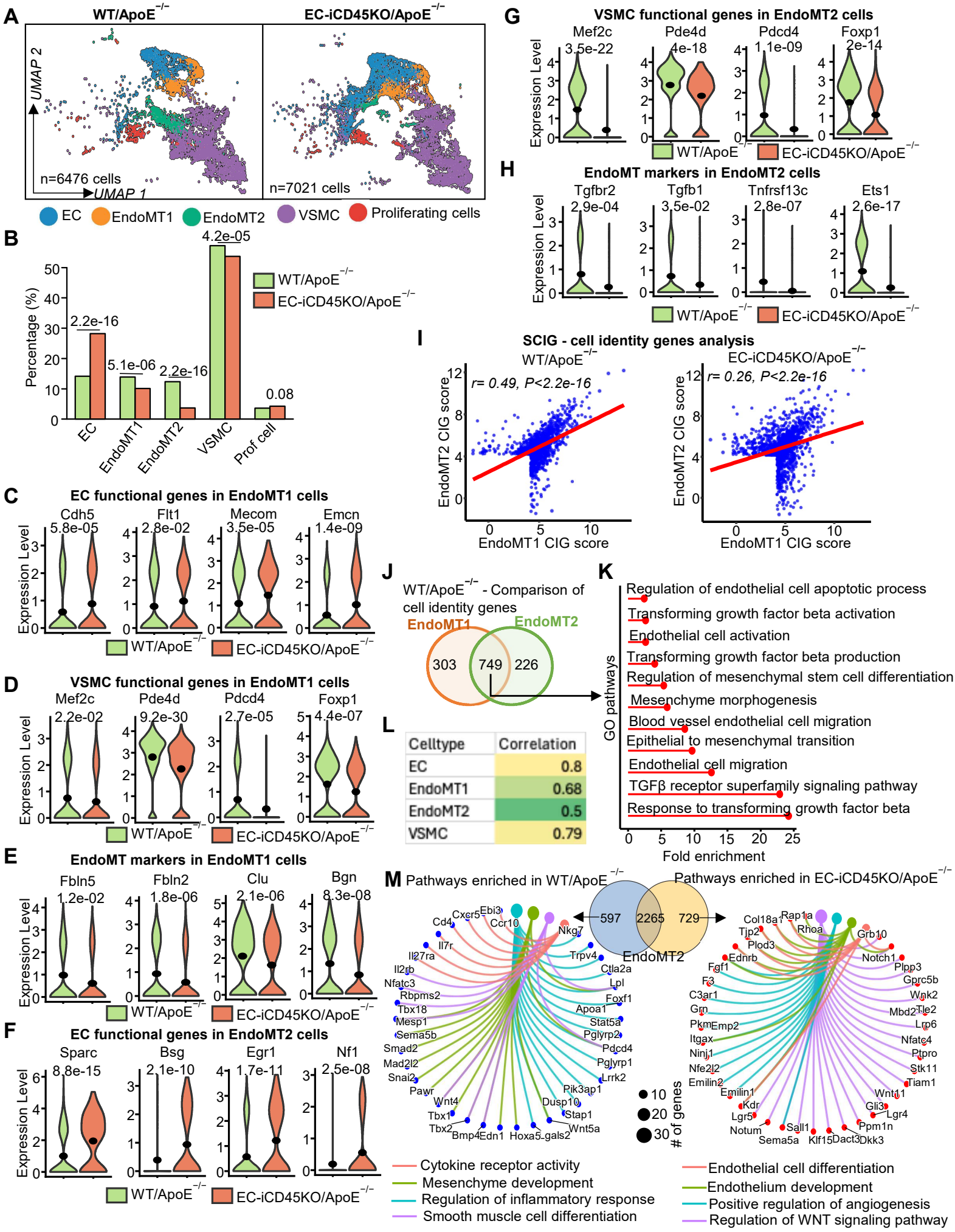
A
WT/ApoE−/−
EC-iCD45KO/ApoE−/−
UMAP 2
UMAP 1
n=6476 cells
n=7021 cells
EC
EndoMT1
EndoMT2
VSMC
Proliferating cells
B
Percentage (%)
WT/ApoE−/−
EC-iCD45KO/ApoE−/−
2.2e-16
5.1e-06
2.2e-16
4.2e-05
0.08
EC
EndoMT1
EndoMT2
VSMC
Prof cell
C
EC functional genes in EndoMT1 cells
Cdh5 5.8e-05
Flt1 2.8e-02
Mecom 3.5e-05
Emcn 1.4e-09
Expression Level
D
VSMC functional genes in EndoMT1 cells
Mef2c 2.2e-02
Pde4d 9.2e-30
Pdcd4 2.7e-05
Foxp1 4.4e-07
E
EndoMT markers in EndoMT1 cells
Fbln5 1.2e-02
Fbln2 1.8e-06
Clu 2.1e-06
Bgn 8.3e-08
F
EC functional genes in EndoMT2 cells
Sparc 8.8e-15
Bsg 2.1e-10
Egr1 1.7e-11
Nf1 2.5e-08
G
VSMC functional genes in EndoMT2 cells
Mef2c 3.5e-22
Pde4d 4e-18
Pdcd4 1.1e-09
Foxp1 2e-14
H
EndoMT markers in EndoMT2 cells
Tgfbr2 2.9e-04
Tgfb1 3.5e-02
Tnfrsf13c 2.8e-07
Ets1 2.6e-17
I
SCIG - cell identity genes analysis
r= 0.49, P<2.2e-16
r= 0.26, P<2.2e-16
EndoMT2 CIG score
EndoMT1 CIG score
J
WT/ApoE−/− - Comparison of cell identity genes
EndoMT1
EndoMT2
303
749
226
K
GO pathways
Regulation of endothelial cell apoptotic process
Transforming growth factor beta activation
Endothelial cell activation
Transforming growth factor beta production
Regulation of mesenchymal stem cell differentiation
Mesenchyme morphogenesis
Blood vessel endothelial cell migration
Epithelial to mesenchymal transition
Endothelial cell migration
TGFβ receptor superfamily signaling pathway
Response to transforming growth factor beta
Fold enrichment
L
Celltype | Correlation
EC | 0.8
EndoMT1 | 0.68
EndoMT2 | 0.5
VSMC | 0.79
M
Pathways enriched in WT/ApoE−/−
Pathways enriched in EC-iCD45KO/ApoE−/−
597
2265
729
EndoMT2
# of genes
Cytokine receptor activity
Mesenchyme development
Regulation of inflammatory response
Smooth muscle cell differentiation
Endothelial cell differentiation
Endothelium development
Positive regulation of angiogenesis
Regulation of WNT signaling pathway

Figure 3

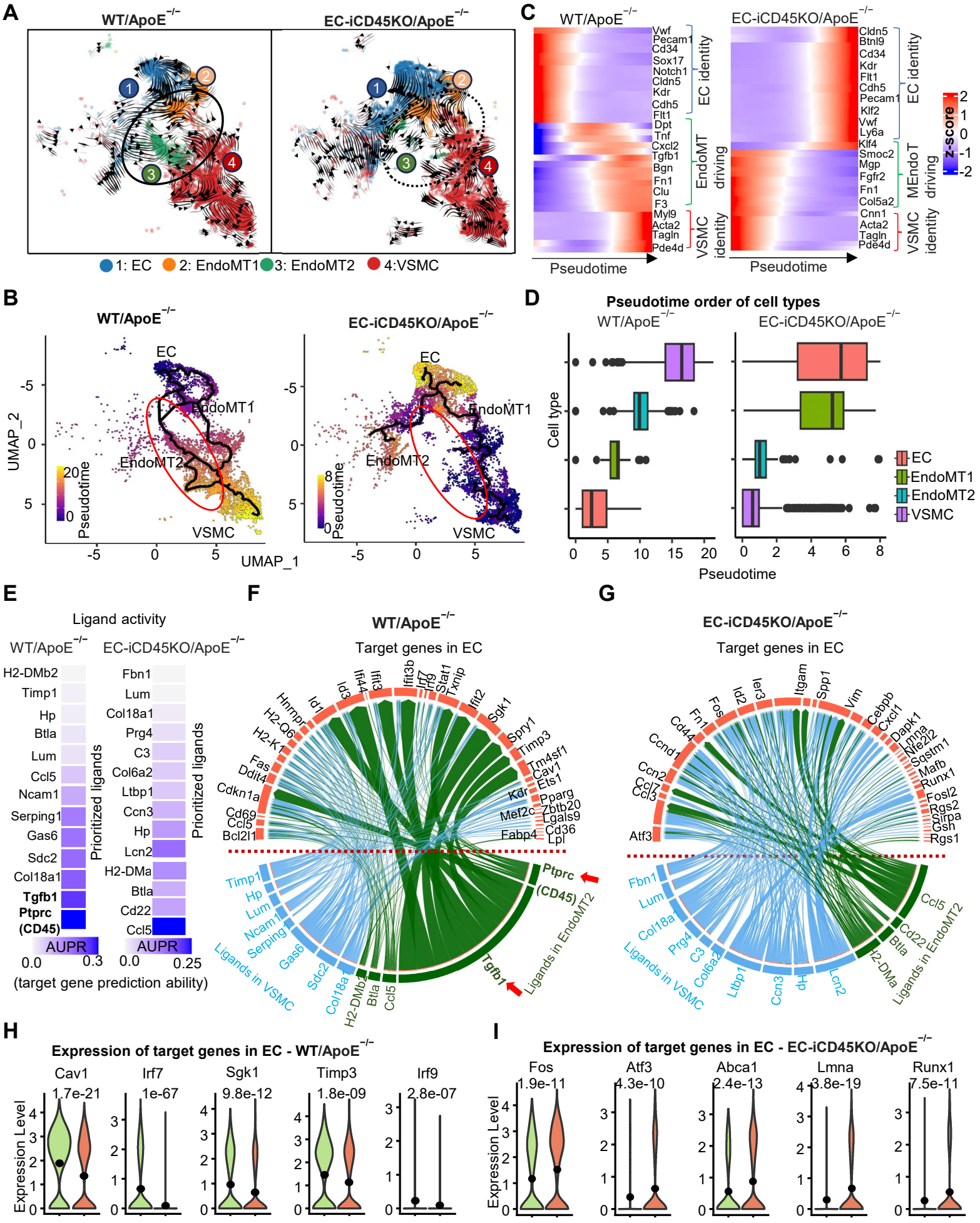
A
WT/ApoE−/−
EC-iCD45KO/ApoE−/−
1: EC
2: EndoMT1
3: EndoMT2
4:VSMC
B
WT/ApoE−/−
EC-iCD45KO/ApoE−/−
EC
EndoMT1
EndoMT2
VSMC
Pseudotime
UMAP_2
UMAP_1
C
WT/ApoE−/−
EC-iCD45KO/ApoE−/−
EC identity
EndoMT driving
VSMC identity
MEndoT driving
Pseudotime
z-score
D
Pseudotime order of cell types
WT/ApoE−/−
EC-iCD45KO/ApoE−/−
Cell type
Pseudotime
EC
EndoMT1
EndoMT2
VSMC
E
Ligand activity
WT/ApoE−/−
EC-iCD45KO/ApoE−/−
Prioritized ligands
AUPR
(target gene prediction ability)
F
WT/ApoE−/−
Target genes in EC
Ligands in EndoMT2
Ligands in VSMC
G
EC-iCD45KO/ApoE−/−
Target genes in EC
Ligands in EndoMT2
Ligands in VSMC
H
Expression of target genes in EC - WT/ApoE−/−
Cav1 1.7e-21
Irf7 1e-67
Sgk1 9.8e-12
Timp3 1.8e-09
Irf9 2.8e-07
Expression Level
I
Expression of target genes in EC - EC-iCD45KO/ApoE−/−
Fos 1.9e-11
Atf3 4.3e-10
Abca1 2.4e-13
Lmna 3.8e-19
Runx1 7.5e-11
Expression Level

Figure 4

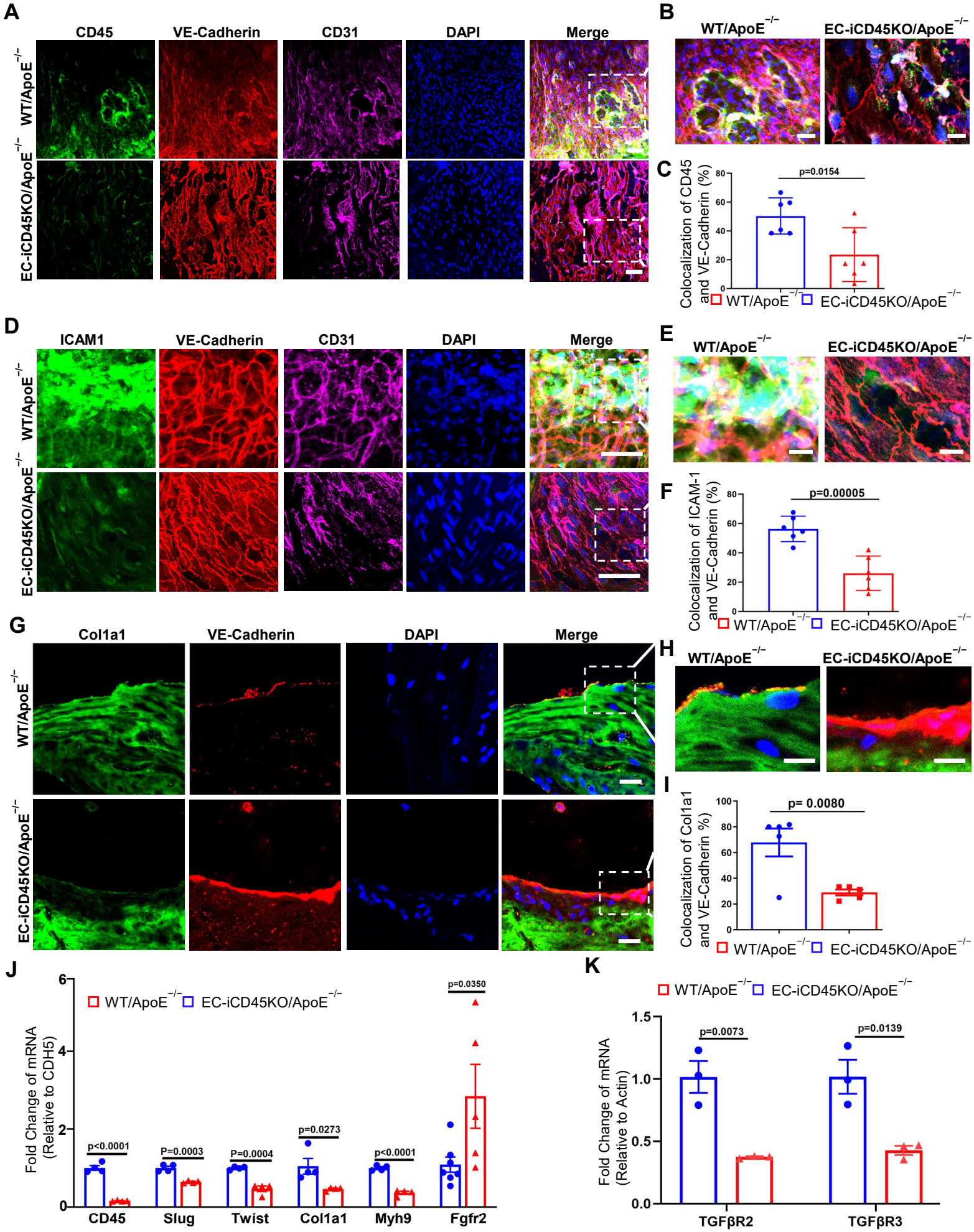
A
CD45
VE-Cadherin
CD31
DAPI
Merge
WT/ApoE−/−
EC-iCD45KO/ApoE−/−
B
WT/ApoE−/−
EC-iCD45KO/ApoE−/−
C
Colocalization of CD45 and VE-Cadherin (%)
p=0.0154
WT/ApoE−/−
EC-iCD45KO/ApoE−/−
D
ICAM1
VE-Cadherin
CD31
DAPI
Merge
WT/ApoE−/−
EC-iCD45KO/ApoE−/−
E
WT/ApoE−/−
EC-iCD45KO/ApoE−/−
F
Colocalization of ICAM-1 and VE-Cadherin (%)
p=0.00005
WT/ApoE−/−
EC-iCD45KO/ApoE−/−
G
Col1a1
VE-Cadherin
DAPI
Merge
WT/ApoE−/−
EC-iCD45KO/ApoE−/−
H
WT/ApoE−/−
EC-iCD45KO/ApoE−/−
I
Colocalization of Col1a1 and VE-Cadherin %)
p= 0.0080
WT/ApoE−/−
EC-iCD45KO/ApoE−/−
J
WT/ApoE−/−
EC-iCD45KO/ApoE−/−
Fold Change of mRNA (Relative to CDH5)
p<0.0001
P=0.0003
P=0.0004
p=0.0273
p<0.0001
p=0.0350
CD45
Slug
Twist
Col1a1
Myh9
Fgfr2
K
WT/ApoE−/−
EC-iCD45KO/ApoE−/−
Fold Change of mRNA (Relative to Actin)
p=0.0073
p=0.0139
TGFβR2
TGFβR3

Figure 5

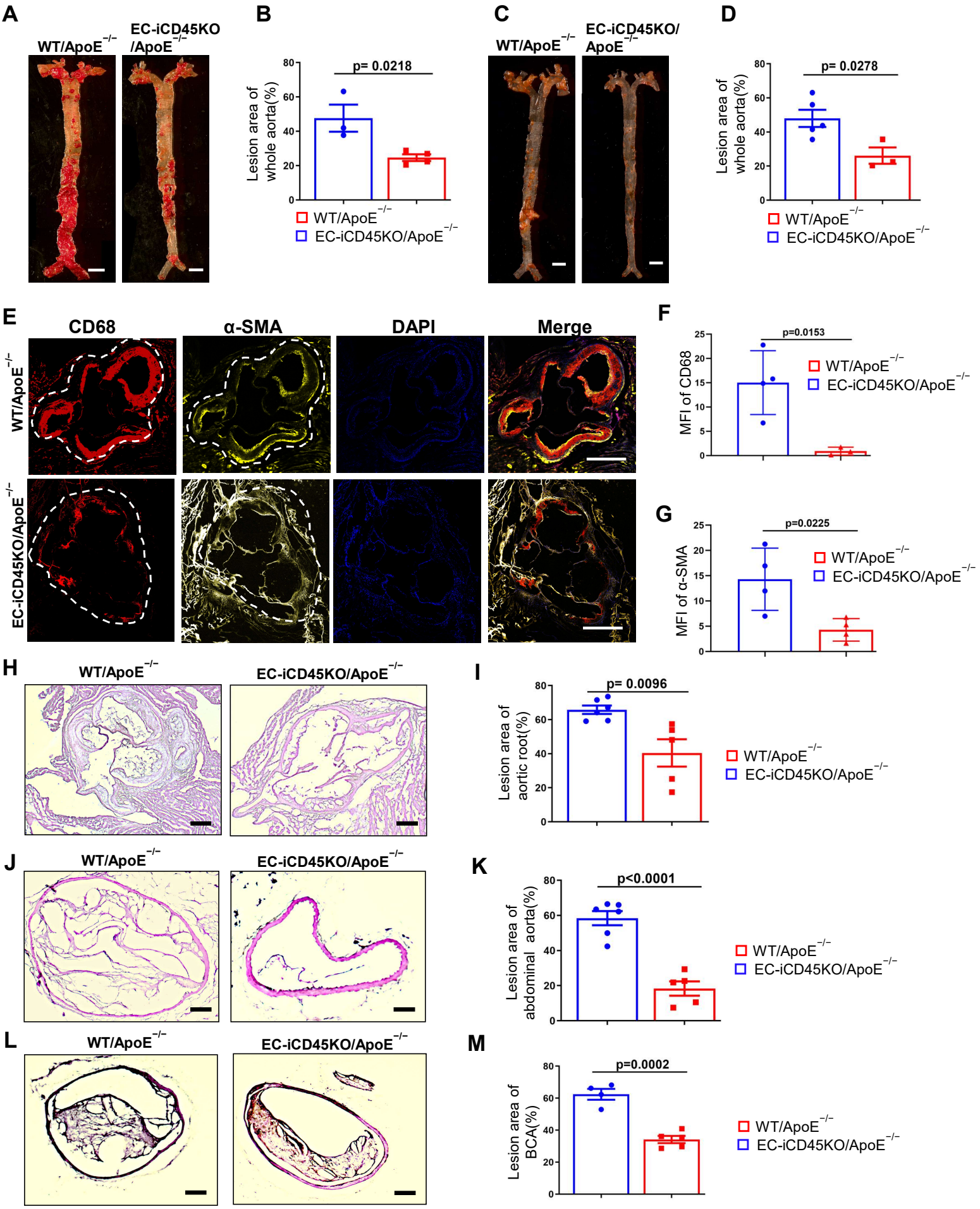
A
WT/ApoE−/−
EC-iCD45KO /ApoE−/−
B
p= 0.0218
Lesion area of whole aorta(%)
WT/ApoE−/−
EC-iCD45KO/ApoE−/−
C
WT/ApoE−/−
EC-iCD45KO/ ApoE−/−
D
p= 0.0278
Lesion area of whole aorta(%)
WT/ApoE−/−
EC-iCD45KO/ApoE−/−
E
CD68
α-SMA
DAPI
Merge
WT/ApoE−/−
EC-iCD45KO/ApoE−/−
F
p=0.0153
MFI of CD68
WT/ApoE−/−
EC-iCD45KO/ApoE−/−
G
p=0.0225
MFI of α-SMA
WT/ApoE−/−
EC-iCD45KO/ApoE−/−
H
WT/ApoE−/−
EC-iCD45KO/ApoE−/−
I
p= 0.0096
Lesion area of aortic root(%)
WT/ApoE−/−
EC-iCD45KO/ApoE−/−
J
WT/ApoE−/−
EC-iCD45KO/ApoE−/−
K
p<0.0001
Lesion area of abdominal aorta(%)
WT/ApoE−/−
EC-iCD45KO/ApoE−/−
L
WT/ApoE−/−
EC-iCD45KO/ApoE−/−
M
p=0.0002
Lesion area of BCA(%)
WT/ApoE−/−
EC-iCD45KO/ApoE−/−

Figure 6

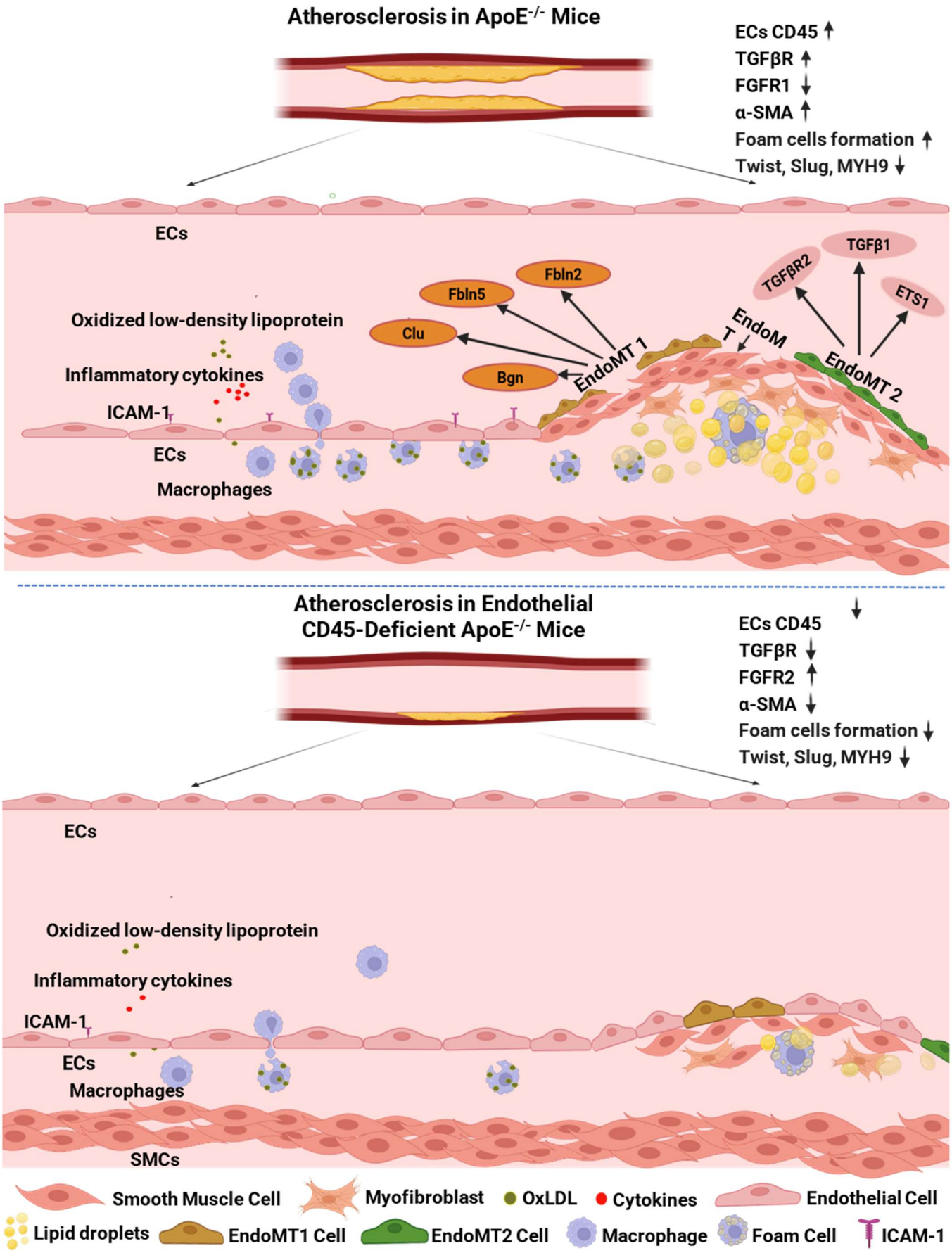
Atherosclerosis in ApoE-/- Mice
ECs CD45 ↑
TGFβR ↑
FGFR1 ↓
α-SMA ↑
Foam cells formation ↑
Twist, Slug, MYH9 ↓
ECs
Oxidized low-density lipoprotein
Inflammatory cytokines
ICAM-1
ECs
Macrophages
Fbln2
Fbln5
Clu
Bgn
EndoMT 1
EndoMT 2
TGFβR2
TGFβ1
ETS1
Atherosclerosis in Endothelial CD45-Deficient ApoE-/- Mice
ECs CD45 ↓
TGFβR ↓
FGFR2 ↑
α-SMA ↓
Foam cells formation ↓
Twist, Slug, MYH9 ↓
ECs
Oxidized low-density lipoprotein
Inflammatory cytokines
ICAM-1
ECs
Macrophages
SMCs
Smooth Muscle Cell
Myofibroblast
OxLDL
Cytokines
Endothelial Cell
Lipid droplets
EndoMT1 Cell
EndoMT2 Cell
Macrophage
Foam Cell
ICAM-1